Journal of Hydrology 568 (2019) 385–402

Contents lists available at ScienceDirect

Journal of Hydrology

journal homepage: www.elsevier.com/locate/jhydrol

Research papers

Revisiting the evolution of the 2009–2011 meteorological drought over Southwest China

Shanlei Sun[a,*], Qingqing Li[a], Jinjian Li[b], Guojie Wang[c], Shujia Zhou[a], Rongfan Chai[a], Wenjian Hua[a], Peng Deng[a], Jie Wang[a], Weiping Lou[d]

[a] Collaborative Innovation Center on Forecast and Evaluation of Meteorological Disasters/Key Laboratory of Meteorological Disaster, Ministry of Education/International Joint Research Laboratory on Climate and Environment Change, Nanjing University of Information Science and Technology (NUIST), Nanjing, China
[b] School of Atmospheric Sciences, Chengdu University of Information Technology, Chengdu, China
[c] School of Geography Sciences, NUIST, Nanjing, China
[d] Xinchang County Meteorological Bureau, Shaoxing, China

ARTICLE INFO

This manuscript was handled by Marco Borga, Editor-in-Chief, with the assistance of Di Long, Associate Editor

Keywords:
Drought processes
Separation method
Standardized Precipitation–Evapotranspiration Index
Climate anomaly
Southwest China

ABSTRACT

With intensifying climate change, droughts over Southwest China (SWC) are drawing increasing interest. The droughts of 2009–2011 have attracted special concern. However, the roles of atmospheric evaporative demand [reflected by reference evapotranspiration (ET_0)] and precipitation (P) anomalies in drought evolutions are still unclear. To that end, we revisited the evolution of the 2009–2011 SWC meteorological droughts quantitatively and comprehensively by quantifying the ET_0 and P impacts. In terms of three drought parameters [i.e., drought intensity (DI), area (DA), and duration (DD)], SWC experienced the second most severe drought of the 1961–2012 period in 2009. Evident differences existed among the drought conditions in different months, i.e., more severe droughts occurred in February–March 2009, September 2009 to March 2010, and June–October 2011. Based on the annual means over drought regions, the 2009 and 2011 DI (DA) could be attributed to lower P, but the P and ET_0 impacts [P, ET_0, and P-and-ET_0 (which reflects drought occurrence due to their combined impacts only)] were comparable in 2010. In addition, P reduction was responsible for DD during 2009–2011. Except in January–March, which were dominated mostly by P, DI (DA) was generally dominated by ET_0 (ET_0 or P-and-ET_0) over the three years. While P dominated spatially and temporally for the majority of the 36 months for DI (DD), some areas were mainly affected by ET_0 (ET_0 or P-and-ET_0). Therefore, to better understand drought evolutions and improve drought monitoring and forecasting, the impacts of ET_0 anomalies should be fully considered. The results of this study provide an important reference framework for comprehensively understanding the underlying mechanisms of droughts not only in SWC but also in other regions around the world.

1. Introduction

Drought, characterized by below-normal water availability over a period from several months to a few decades, is a complex, important, and recurrent extreme climate event for a region (Dai, 2011; Sheffield et al., 2012). A drought usually exerts negative and far-reaching impacts on social, economic, and environmental sectors. Droughts accompanied by heat waves are estimated to have cost around $210.1 billion (U.S.) during 1980–2011 (Ganguli and Ganguly, 2016). The 2008–2009 winter drought in northeastern China, one of the worst droughts in the past 50 years, resulted in more than 10 million people lacking drinking water and economic losses of nearly $2.3 billion (Wang et al., 2011). Drought is regarded as one of the most damaging natural disasters (Wilhite, 2000) and is a perennial concern for the public and governments across the globe. In recent decades in particular, droughts have occurred more frequently, with greater intensities and longer durations, and have affected larger spatial areas, possibly due to intensifying climate change (Sheffield et al., 2012; Dai, 2013; IPCC, 2014; Trenberth et al., 2014; Williams et al., 2015). Therefore, the spatiotemporal characteristics, underlying mechanisms, and related impacts of droughts have been receiving increasing attention on both regional and global scales. Examples include the spatiotemporal trends of droughts in the U.S. (Ganguli and Ganguly, 2016), China (Yu et al., 2014), and Europe (Spinoni et al., 2017); the linkage between droughts and atmospheric anomaly-induced precipitation (P) reduction in Central Equatorial Africa (Hua et al., 2017), California (Seager et al., 2015),

* Corresponding author at: International Joint Laboratory on Climate and Environment Change, Nanjing University of Information Science & Technology (NUIST), Ningliu Road 219, Nanjing 210044, China.
E-mail address: ppsunsanlei@126.com (S. Sun).

https://doi.org/10.1016/j.jhydrol.2018.10.071
Received 14 May 2018; Received in revised form 26 October 2018; Accepted 30 October 2018
Available online 10 November 2018
0022-1694/ © 2018 Elsevier B.V. All rights reserved.

and southern China (Lu et al., 2011); the impacts of atmospheric evaporative demand [AED, which can be reflected by potential (PET) or reference evapotranspiration (ET_0)] changes on droughts in California (Williams et al., 2015; Diffenbaugh et al., 2015) and worldwide (Dai, 2013); and drought impacts on the U.S. ecosystem (Sun et al., 2015) and the water–energy nexus in Texas (Scanlon et al., 2013).

Various natural disasters and drought in particular have affected China frequently. Between 1949 and 2013, an average of approximately 2.1×10^5 km^2 of cropland—accounting for nearly 16.7% of the total arable area—was impacted by drought annually (Zhai et al., 2017). Droughts can happen anywhere (in regions with more or less climatological P) and anytime (in wet or dry months); however, due to differences in climatological backgrounds and climate change, drought variations (i.e., intensity, duration, frequency, and extent) differ from region to region (Zou et al., 2005; She and Xia, 2013; Wang and Chen, 2012; Huang et al., 2015; Choi et al., 2016; Ma et al., 2016; Wang et al., 2015a,b; Zhang et al., 2016, 2017a). For example, using the Palmer drought severity index (PDSI), Choi et al. (2016) showed that the drought intensity in North China strengthened throughout all seasons during 1979–2005, especially in the summer and fall. In recent decades, the Yellow River has remained below normal levels for long periods of time (She and Xia, 2013), and zero flow has even happened regularly in its lower reaches since the 1970s, which implies high drought risk in the Yellow River Basin (Huang et al., 2015; Ma et al., 2016). Wang et al. (2015a,b) employed the Standardized Precipitation–Evapotranspiration Index (SPEI) to explore drought evolution from 1960 to 2010 in Northwest China (a typically arid region) and determined that the region had become wetter on both annual and seasonal scales. Despite no obvious changes occurring in the PDSI for the entire Yangtze River Basin during 1961–2005, the middle (the lower and upper) part(s) of this basin exhibited statistically significant downward (upward) trend (Zhai et al., 2010).

With drought aggravation in the northern (traditionally arid) regions of China, the southern and eastern (wet) regions have experienced more frequent and more severe (e.g., higher-intensity and more widespread) droughts since the beginning of the 21st century (Liu et al., 2012). For example, severe droughts occurred in Sichuan (SC) Province in the autumns of 2004 and 2007, despite there being thousands of rivers within this region; a once-in-a-century drought occurred in 2006 in Chongqing (CQ); and a severe and prolonged drought occurred from the autumn of 2009 to the spring of 2010 in Southwest China (SWC). Among these, the 2009–2010 drought in SWC was believed to be a record-breaking event from the perspective of historical meteorological observations. During this drought, most rivers shrank to 30–80% of their normal volumes, and some even dried up completely. Approximately 21 million people lacked drinking water, and economic losses reached nearly $30 billion (Lu et al., 2011, 2014; Yang et al., 2012a,b). Because of the far-reaching and devastating impacts of this drought throughout SWC, the Chinese government and academic researchers (e.g., meteorologists, hydrologists, agriculturalists, ecologists, and economists) have paid particular attention to this event. Moreover, there is general agreement that drought occurrence in SWC has become more frequent and intense during the past 50 years and that these trends will continue in the future (Wang and Chen, 2012; Wang et al., 2014a,b, 2015a,b). Thus, to better mitigate increasing drought risks and reduce drought-induced losses in SWC, it is urgent and critically important to analyze the spatiotemporal evolution of drought and its relevant underlying mechanisms comprehensively. Considering the close association between P (the major water supply component) and drought, numerous scholars have worked to identify possible causes of negative P anomalies based on drought generalities and case studies (Li et al., 2009; Xu et al., 2012; Huang et al., 2012; Yang et al., 2012a,b; Zhang et al., 2013a,b, 2014; Wang et al., 2015a,b; Liu et al., 2017a,b). Yang et al. (2012a,b) found that SWC P was significantly and positively correlated with the Arctic Oscillation (AO) index, which suggests that a negative AO phase might correspond to drought in this region. Xu et al. (2012) stated that, despite a significant positive relationship between the North Atlantic Oscillation (NAO) and SWC P in boreal winter, the NAO asymmetrically impacted P, i.e., the NAO negative phase could clearly generate a P deficiency, but the positive phase could only induce limited increases in P. Zhang et al. (2013a,b) noted that the concurrent distinctive warm pool during El Niño could have created a strongly anomalous cyclone over the western North Pacific, resulting in a serious reduction in SWC P (a severe drought) in the autumn of 2009. Liu et al. (2017a,b) suggested that severe summer and early fall droughts in SWC occurred mainly due to negative water vapor transport anomalies from the Indo-China Peninsula channel.

It is worth noting that the vast majority of studies on SWC droughts have focused on P anomalies and their associated mechanisms, paying little or no attention to the effects of AED. Depending on the soil water balance, AED can play an important role in soil water losses (Hobbins et al., 2008), which are intimately related to dryness/wetness and drought variations. Furthermore, this close relationship has been confirmed around the world (Hu and Willson, 2000; Dai, 2013; IPCC, 2014; Williams et al., 2015; Shukla et al., 2015; Diffenbaugh et al., 2015; Sun et al., 2017a), with some researchers warning that ignoring the influence of AED may result in uncertainties for knowing drought variations, physical mechanisms, and projected future drought conditions (Wang and Chen, 2012; Teuling et al., 2013; Xu et al., 2015; Sun et al., 2017a). In response to global warming, significant changes in various climate elements (e.g., temperature, humidity, sunshine duration (SSD), and wind speed] have been detected over SWC (Qin et al., 2010; Yang et al., 2012a,b; Li et al., 2012; Mao et al., 2015), resulting in ET_0 variations (Fan and Thomas, 2013; Sun et al., 2017b,c). In view of the longer duration, larger extent, and higher intensity of the 2009–2011 droughts, which had far-reaching negative consequences for the region's environment and various socioeconomic sectors, a number of studies have been conducted on these events using a variety of drought indices (e.g., Yang et al., 2012a,b; Yan et al., 2013; Long et al., 2014; Wang et al., 2014a,b; Cui et al., 2015; Liu et al., 2016, 2017a,b).

While these studies have led to improved understanding of drought processes, two major unresolved issues remain: (1) the role that AED plays in the spatiotemporal evolution of drought, and (2) whether droughts are always dependent on P anomalies. To address these questions, we revisited the 2009–2011 SWC meteorological drought evolutions comprehensively and quantitatively by considering the effects of P and AED (reflected by ET_0 in this study). The major objectives of this study were as follows: (1) to analyze the values of annual and monthly drought parameters (i.e., drought intensity, duration, and extent) during 2009–2011, based on a three-month SPEI (SPEI-3); (2) to quantify the respective contributions of anomalous P and ET_0, based on several sensitivity experiments and a separation method proposed by Sun et al. (2014, 2017b); and (3) to address the two unresolved issues in the aforementioned analyses. The results of this study allow us to better understand meteorological drought evolutions in response to climate anomalies over SWC.

2. Data and methodology

2.1. Study region

This study region of SWC (between 21 and 34°N and 97–110°E) mainly includes SC, CQ, Guizhou (GZ), Yunnan (YN), and the western part of Guangxi (wGX) Province. It encompasses a large geographic area with complex landscapes, e.g., the plateau of YN-GZ and western SC, the eastern SC Hills, the Hengduan Mountains, and the SC Basin. A typical subtropical monsoon climate prevails across SWC, with a clearly defined dry/wet season. Over this region, regional mean monthly P increases quickly starting in April, peaks in July, and sharply decreases afterward. For the monthly ET_0, the regional mean has two peaks in May and July. During 1961–2012, the annual P (ET_0) is > 1000 mm (980 mm) and shows large spatial differences with a range from >

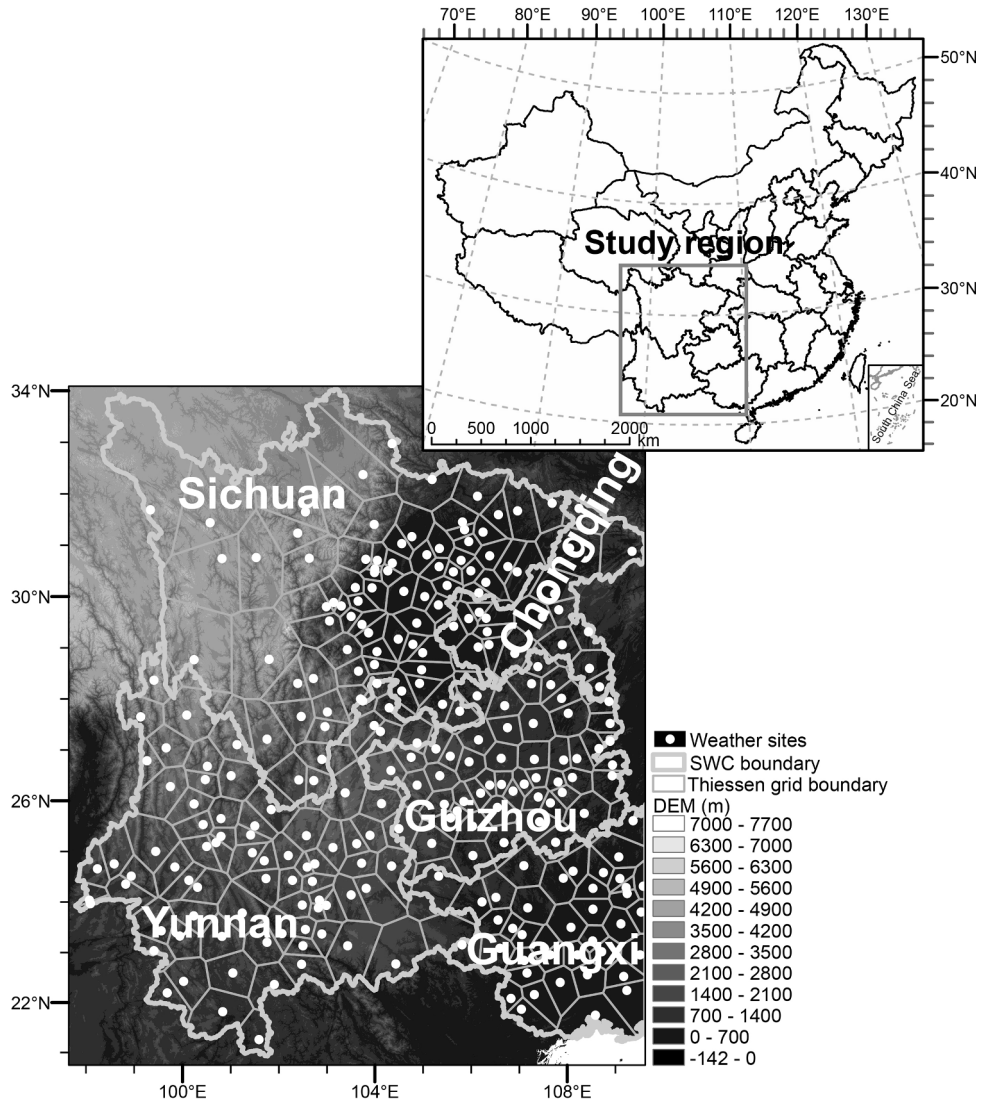

Fig. 1. Location of SWC with 269 weather observation sites (or Thiessen grids). The digital elevation model (DEM) with a spatial resolution of 90 m is available at: http://srtm.csi.cgiar.org/.

700 mm (900 mm) in western SC (northeastern SWC) to < 1400 mm (1000 mm) in wGX (YN).

2.2. Data

For computing the Penman–Monteith ET_0 (Allen et al., 1998) and the SPEI (Vicente-Serrano et al., 2010) and conducting sensitivity experiments, we collected monthly meteorological datasets from the China Meteorological Administration (CMA), mainly including P (mm); mean, maximum, and minimum air temperatures (°C); 10-m wind speed (m/s); SSD (h/mon); and relative humidity (%). The datasets span 1960–2012 with observations at 334 sites. Before using the data, two data quality issues of inhomogeneity and missing values were resolved. First, the *Pettitt* test is employed to check the time series homogeneity (Wijngaard et al., 2003), and variables that cannot pass the significance test ($p < 0.05$) are eliminated. Subsequently, the sites with data available for fewer than 10 months each year are also removed; the missing values in the records of the other stations are filled using the data from nearby sites with a linear regression. After this quality control process, data from 269 sites remained (Fig. 1). Considering the spatially uneven features of these sites, which potentially introduce uncertainties into the results (e.g., the regional mean), the Thiessen polygon method is employed for obtaining the area represented by each site (Fig. 1).

In addition, the daily NCEP/NCAR Reanalysis-1 (Kalnay et al., 1996) dataset during 1960–2012, including wind speed and specific humidity, is utilized. These data are used to calculate the monthly column-integrated water vapor flux from the surface to 300 hPa and divergence during 2009–2011 and their corresponding monthly anomalies relative to the multi-year (1961–2012) mean. Through comparing the monthly anomalies of P against those of water vapor flux and divergence, the possible causes of negative P anomalies will be briefly discussed from perspective of the atmospheric circulation patterns.

2.3. Methodology

2.3.1. Computing ET_0 and SPEI-3

To date, hundreds of approaches for determining AED have been proposed (Xu and Singh, 2001), including the use of a water budget (e.g., Guitjens, 1982), mass transfer (e.g., Harbeck, 1962), radiation-based approaches (e.g., Priestley and Taylor, 1972), temperature-based approaches (e.g., Thornthwaite, 1948) and combinations of these other approaches (e.g., Penman and Penman–Monteith; Allen et al., 1998; Liu et al., 2018). The Penman–Monteith equation considers various climatic variables, i.e., temperature, water vapor deficit, SSD (or net radiation),

Table 1
Detailed information about the numerical experiments.

Experiments	Description
SPEI_Ctl	Monthly P, *SSD*, *Tave*, U_2 and *Rh* during 1960–2012
SPEI_non-P	For each month, P fixed at its 52-year (1961–2012) climatological mean; monthly *SSD*, *Tave*, U_2 and *Rh* during 1960–2012
SPEI_non-SSD	For each month, *SSD* fixed at its 52-year (1961–2012) climatological mean; monthly P, *Tave*, U_2 and *Rh* during 1960–2012
SPEI_non-Tave	For each month, *Tave* fixed at its 52-year (1961–2012) climatological mean; monthly *SSD*, P, U_2 and *Rh* during 1960–2012
SPEI_non-U_2	For each month, U_2 fixed at its 52-year (1961–2012) climatological mean; monthly *SSD*, *Tave*, P and *Rh* during 1960–2012
SPEI_non-Rh	For each month, *Rh* fixed at its 52-year (1961–2012) climatological mean; monthly *SSD*, *Tave*, U_2 and P during 1960–2012

and wind speed, which suggests that this method incorporates a comprehensive physical concept of evapotranspiration processes. To better reflect the effects of climate anomalies on AED, as well as SPEI-3 or drought, we used an equation of the Penman–Monteith type (i.e., the Food and Agriculture Organization of the United Nations (FAO)-56 equation; Allen et al., 1998) to estimate ET_0 for representing AED. This equation is written as follows:

$$ET_0 = \frac{0.408\Delta(R_n - G) + \gamma\frac{900}{Tave+273}U_2 e_s(1 - Rh)}{\Delta + \gamma(1 + 0.34U_2)}, \quad (1)$$

where *Rn* [MJ/(m^2 d)] is the net radiation at the surface, which is closely related to SSD (detailed computations are shown in Supplementary Text S1); *G* (MJ/(m^2 d)) is the soil heat flux density, which can be ignored at monthly or longer scales; γ (kPa/°C) and Δ (kPa/°C) are the psychometric constant and the rate of change in vapor pressure with temperature, respectively; U_2 (m/s) is the 2-m wind speed converted from the 10-m wind speed; *Rh* (%) and e_s (kPa) are the relative humidity and saturation vapor pressure, respectively; and *Tave* (°C) is the mean temperature. More information about γ, Δ, e_s, and U_2 computations can be found in Allen et al. (1998).

Using drought statistics from various yearbooks of meteorological disasters, Wang and Chen (2012) evaluated results from the SPEI model for SWC and found that this index could reproduce the principal meteorological drought features in this region well. Therefore, this index was chosen to represent dryness/wetness in SWC and to determine the values of drought parameters. SPEI, which is based on the Standardized Precipitation Index (SPI; McKee et al., 1993), was proposed by Vicente-Serrano et al. (2010). It is easy to calculate and can flexibly track dry/wet events on various time scales. Monthly P and ET_0 data are usually necessary to calculate the climatic water balance ($D = P - ET_0$) for a certain month before they are aggregated at various time scales. A three-parameter log-logistic distribution is recommended to fit the D time series for each month. An inverse normal function is then used to standardize the probabilities (Vicente-Serrano et al., 2010). In a certain region, negative and positive SPEI values typically indicate dry and wet conditions, respectively. In this study, we focused on short- and medium-term meteorological droughts, which are closely associated with agricultural droughts as defined by soil moisture (Hao and Singh, 2015; Wu et al., 2015). In our preliminary work (not shown here), we calculated the correlation coefficients (*Rs*) of the 1-, 3-, 6-, 9-, and 12-month SPEI with GLADAS2.0-Noah (Global Land Data Assimilation System version 2.0 with the Noah model) soil moisture anomalies over SWC on a monthly scale and found that the SPEI-3 corresponded to the largest *R*, which suggests that the SPEI-3 best represents agricultural drought over SWC. Thus, the SPEI-3 was selected for further analyses. Monthly ET_0 and SPEI-3 time series during 1961–2012 were calculated for 269 sites in SWC, and then annual P and ET_0 (SPEI-3) values were obtained by summing (averaging) the monthly values for each year.

2.3.2. Separating the respective contributions of P and ET_0 to SPEI-3 anomalies

It is difficult to separate the respective contributions of P and ET_0 to SPEI-3 anomalies because of the compounding effects of these driving factors' interactions. To resolve this issue, Sun et al. (2014, 2017b) proposed a new separation method based on several sensitivity experiments. This method has been employed for attributing linear trends in streamflow and evapotranspiration in the Poyang Lake Basin of China and ET_0 in SWC. Notably, the original version of the method was developed to quantify the individual contributions of each factor to the linear trends in hydrometeorological parameters. Thus, we have improved this method to satisfy this study's aims of differentiating between the contributions of P and ET_0 to annual and monthly SPEI-3 anomalies. Two validation metrics (i.e., *R* and scatter-plots) were selected to evaluate the performance of this improved approach. Details of the results are presented in Section 3.2.1.

Like the separation method proposed by Sun et al. (2014, 2017b), the method developed in this study involves two major procedures, i.e., reasonable sensitivity experiments (Table 1) and an efficient algorithm [Eqs. (2) and (3)] for determining the individual contribution of each factor. Six (i.e., one control and five sensitivity) experiments were designed and conducted with the SPEI model. The control experiment (SPEI_Ctl) was run with all of the original climate variables (i.e., remaining intra- and inter-annual fluctuations) during 1960–2012 as inputs; however, for the *I*th sensitivity experiment (SPEI_non-I), the inputs for the 52-year (1961–2012) climatological mean of the *I*th factor for each month (i.e., only the remaining intra-annual fluctuation) and the original monthly time series of the other four factors during 1960–2012 were used. The sensitivity experiments for P, *SSD*, *Tave*, U_2, and *Rh* are referred to here as SPEI_non-P, SPEI_non-SSD, SPEI_non-Tave, SPEI_non-U_2, and SPEI_non-Rh, respectively. Given that differences in the log-logistic probability distribution parameters exist among these six experiments and thus introduce uncertainties into the results, the estimated parameters of the SPEI model from SPEI_Ctl were utilized in running the five sensitivity experiments. Monthly SPEI-3 anomalies for each experiment were obtained by subtracting the 52-year mean. Taking SPEI_non-I as an example, an equation was established based on the hypothesis that SPEI anomalies are caused by the remaining factors except for the *I*th factor, represented as follows:

$$\sum_{K \neq i}^{N} C_{i,k,j}^{K} = V_{i,k,j}^{SPEI_non-I}, \quad (2)$$

where $\sum_{K \neq i}^{N} C_{i,k,j}^{K}$ is the total contribution to the monthly SPEI_non-I SPEI-3 anomalies at the *i*th grid during the *j*th month of the *k*th year, *N* is the number of sensitivity experiments (= 5 here), and $V_{i,k,j}^{SPEI_non-I}$ is the monthly SPEI-3 anomalies from the SPEI_non-I experiment at the *i*th grid during the *j*th month of the *k*th year. We thus obtained a set of simultaneous equations, including five unknown numbers (i.e., $C_{i,k,j}^{P}$, $C_{i,k,j}^{SSD}$, $C_{i,k,j}^{Tave}$, $C_{i,k,j}^{U_2}$, and $C_{i,k,j}^{Rh}$). By solving these equations, the contribution of the *I*th factor at the *i*th grid during the *j*th month of the *k*th year can be computed as follows:

$$C_{i,k,j}^{K} = \frac{\sum_{K \neq i}^{N} V_{i,k,j}^{SPEI_non-K} - (N-2)V_{i,k,j}^{SPEI_non-I}}{N-1}. \quad (3)$$

In this study, the ET_0 contribution to SPEI-3 anomalies was represented as the sum of the respective contributions of *SSD*, *Tave*, U_2, and *Rh*. Additionally, the separation method described above was employed to quantify the impacts of *SSD*, *Tave*, *Rh*, and U_2 on annual and monthly ET_0 anomalies in drought regions. However, it should be noted

that the corresponding designations of experiments are different than those for drought attributions. Details are shown in Table S1.

2.3.3. Quantifying climate anomaly impacts on drought parameters

2.3.3.1. Identifying drought parameters in real time. A threshold is required to determine whether a given month experiences drought at a certain Thiessen grid. In this study, the drought threshold was set to ≤ -1.0. If the monthly SPEI-3 is ≤ -1.0 in a given month, drought occurs, and vice versa. Therefore, we were able to extract the values of drought parameters [i.e., drought intensity (DI), area (DA), and duration (DD)] from the SPEI_Ctl results as follows:

$$\begin{cases} DI_{i,k,j} = SPEI_{i,k,j} \quad (if\ {}^{SPEI_Ctl}SPEI_{i,k,j} \leqslant -1.0) \\ \begin{cases} DI_{SWC,k,j} = \sum_{i=1}^{269} \frac{DI_{i,k,j}A_i y_{i,k,j}}{A_{SWC}} \\ A_{SWC} = \sum_{i=1}^{269} A_i \\ y_{i,k,j} = 1 \quad (if\ {}^{SPEI_Ctl}SPEI_{i,k,j} \leqslant -1.0) \\ y_{i,k,j} = 0 \quad (if\ {}^{SPEI_Ctl}SPEI_{i,k,j} > -1.0) \end{cases} \\ DI_{i,k} = \sum_{j=1}^{12} \frac{DI_{i,k,j}}{12} \\ DI_{SWC,k} = \sum_{j=1}^{12} \frac{DI_{SWC,k,j}}{12} \end{cases} \tag{4}$$

$$\begin{cases} DA_{k,j} = \sum_{i=1}^{269} \frac{A_i y_{i,k,j}}{A_{SWC}} \\ DA_k = \sum_{j=1}^{12} DA_{k,j} \end{cases} \tag{5}$$

$$\begin{cases} DD_{i,k} = \sum_{i=1}^{269} y_{i,k,j} \\ DD_{SWC,k} = \sum_{j=1}^{12} \frac{DD_{i,k}A_i}{A_{SWC}} \end{cases} \tag{6}$$

where $DI_{i,k,j}$ and ${}^{\text{SPEI_Ctl}}SPEI_{i,k,j}$ are DI and SPEI_Ctl SPEI-3, respectively, in the *j*th month of the *k*th year at the *i*th grid; $DI_{SWC,k,j}$ is the SWC regional mean DI in the *j*th month of the *k*th year; $DI_{i,k}$ and $DD_{i,k}$ are the annual DI and DD, respectively, at the *i*th grid in the *k*th year; $DI_{SWC,k}$ ($DD_{SWC,k}$) is the SWC regional mean DI (DD) in the *k*th year; $DA_{k,j}$ is the DA in the *j*th month of the *k*th year; DA_k is the annual total DA in the *k*th year; and A_{SWC} is the area of SWC. Based on the above equations and SPEI_Ctl SPEI-3, monthly and annual drought characteristics were identified for further analyses of drought conditions during 2009–2011.

2.3.3.2. Quantifying climate anomaly impacts. Considering our major objective of determining climate anomaly impacts on drought characteristics in real time, we focused on drought regions during a specific month, which could be identified by SPEI_Ctl SPEI-3 ≤ -1.0 with Eq. (5) and could thus be represented as a condition of "if SPEI_Ctl $SPEI_{i,k,j} \leq -1.0$." The quantitative impacts of P or ET_0 on *DI* were estimated as follows:

$$\begin{cases} {}^{x}CDI_{i,k,j} = {}^{x}C_{i,k,j} \quad (if\ {}^{SPEI_Ctl}SPEI_{i,k,j} \leqslant -1.0) \\ {}^{x}CDI_{i,k} = \sum_{j=1}^{12} \frac{{}^{x}C_{i,k,j}}{12} \\ {}^{x}CDI_{SWC,k,j} = \sum_{i=1}^{269} \frac{{}^{x}CDI_{i,k,j}A_i y_{i,k,j}}{A_{SWC}} \\ {}^{x}CDI_{SWC,k} = \sum_{j=1}^{12} \frac{{}^{x}CDI_{SWC,k,j}}{12} \end{cases} \tag{7}$$

where ${}^{x}CDI_{i,k,j}$ (${}^{x}CDI_{SWC,k,j}$) is the contribution of the *x* (= P or ET_0) anomaly to *DI* at the *i*th grid (SWC) in the *j*th month of the *k*th year and ${}^{x}CDI_{i,k}$ (${}^{x}CDI_{SWC,k}$) is the contribution of the *x* anomaly at the *i*th grid (SWC) in the *k*th year. By comparing the magnitudes of the P and ET_0 contributions, the dominant contributors can be divided into two types, i.e., with P (ET_0) being dominant with larger magnitudes.

In contrast to DI attribution, DA and DD are closely associated with whether monthly precipitation or ET_0 anomaly alone triggers drought [namely, whether the effect of P or ET_0 alone plus the multi-year mean (1961–2012) monthly SPEI_Ctl SPEI-3 is ≤ 1.0]. Therefore, based on the separate contributions of P and ET_0 alone on monthly SPEI-3 anomalies, we were able to reconstruct a new monthly SPEI-3 time series by summarizing the multi-year mean monthly SPEI_Ctl SPEI-3 and P ($SPEI_P_{only}$; ET_0, $SPEI_ET_{0only}$) contribution, which only reflects the P (ET_0) impact. Then, several possible conditions were established. Specifically, for a given drought month (i.e., SPEI_Ctl SPEI-3 ≤ 1.0) on a certain grid, (1) drought disappears in the $SPEI_P_{only}$ and $SPEI_ET_{0only}$ scenarios because SPEI-3 > -1.0; thus, drought occurrence can be attributed to the summarized contributions of P and ET_0; (2) drought exists in the $SPEI_P_{only}$ ($SPEI_ET_{0only}$) scenario rather than in the $SPEI_ET_{0only}$ ($SPEI_P_{only}$) scenario; thus, P (ET_0) is regarded as the major contributor to drought occurrence; (3) drought occurs in the $SPEI_P_{only}$ and $SPEI_ET_{0only}$ scenarios, which suggests that the impacts from P or ET_0 alone can induce drought. Consistently, we can define the determinants as four types: P-and-ET_0, P, ET_0, and P-or-ET_0. These four determinants' contributions to *DD* and *DA* can be estimated as follows:

$$\begin{cases} \begin{cases} {}^{x}CDD_{i,k} = \sum_{j=1}^{12} X_{i,j,k} \\ {}^{x}CDA_{k,j} = \sum_{i=1}^{269} \frac{X_{i,j,k}A_i}{A_{SWC}} \\ {}^{x}CDD_{SWC,k} = \sum_{i=1}^{269} \frac{{}^{x}CDD_{i,k}A_i}{A_{SWC}} \\ {}^{x}CDA_k = \sum_{j=1}^{12} {}^{x}CDA_{k,j} \end{cases} \\ Conditions\ for\ dominant\ of\ P\text{: } X_{i,j,k} = 1, \\ if \begin{cases} {}^{SPEI_Ctl}SPEI_{i,k,j} \leqslant -1.0 \\ {}^{SPEI_P_{only}}SPEI_{i,k,j} \leqslant -1.0 \\ {}^{SPEI_ET_{0only}}SPEI_{i,k,j} > -1.0 \end{cases} ;\ or\ X_{i,j,k} = 0 \\ Conditions\ for\ dominant\ of\ ET_0\text{: } X_{i,j,k} = 1, \\ if \begin{cases} {}^{SPEI_Ctl}SPEI_{i,k,j} \leqslant -1.0 \\ {}^{SPEI_P_{only}}SPEI_{i,k,j} > -1.0 \\ {}^{SPEI_ET_{0only}}SPEI_{i,k,j} \leqslant -1.0 \end{cases} ;\ or\ X_{i,j,k} = 0 \\ Conditions\ for\ dominant\ of\ P-and-ET_0\text{: } X_{i,j,k} = 1, \\ if \begin{cases} {}^{SPEI_Ctl}SPEI_{i,k,j} \leqslant -1.0 \\ {}^{SPEI_P_{only}}SPEI_{i,k,j} > -1.0 \\ {}^{SPEI_ET_{0only}}SPEI_{i,k,j} > -1.0 \end{cases} ;\ or\ X_{i,j,k} = 0 \\ Conditions\ for\ dominant\ of\ P-or-ET_0\text{: } X_{i,j,k} = 1, \\ if \begin{cases} {}^{SPEI_Ctl}SPEI_{i,k,j} \leqslant -1.0 \\ {}^{SPEI_P_{only}}SPEI_{i,k,j} \leqslant -1.0 \\ {}^{SPEI_ET_{0only}}SPEI_{i,k,j} \leqslant -1.0 \end{cases} ;\ or\ X_{i,j,k} = 0 \end{cases} \tag{8}$$

where ${}^{x}CDD_{i,k}$ (${}^{x}CDD_{SWC,k}$) represents the contribution of *x* (= P, ET_0, P-and-ET_0, or P-or-ET_0) at the *i*th grid (SWC) *DD* in the *k*th year; ${}^{x}CDA_{k,j}$ is the contribution of *x* in the *j*th month of the *k*th year; ${}^{x}CDA_k$ is the contribution of *x* in the *k*th year; and ${}^{\text{SPEI_Ponly}}SPEI_{i,k,j}$ and

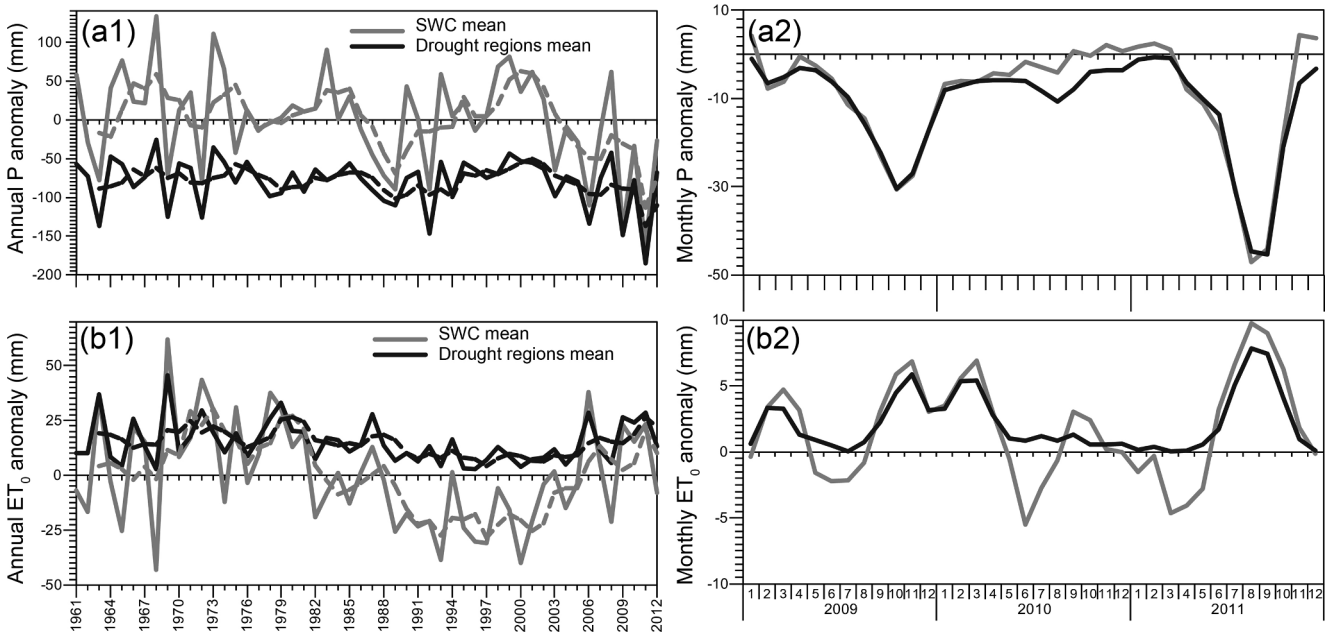

Fig. 2. P and ET_0 anomalies at annual (a1 and b1) and monthly (a2 and b2) scales for the periods of 1961–2012 and 2009–2011, respectively. In (a1) and (b1), the dashed line represents the three-year running mean.

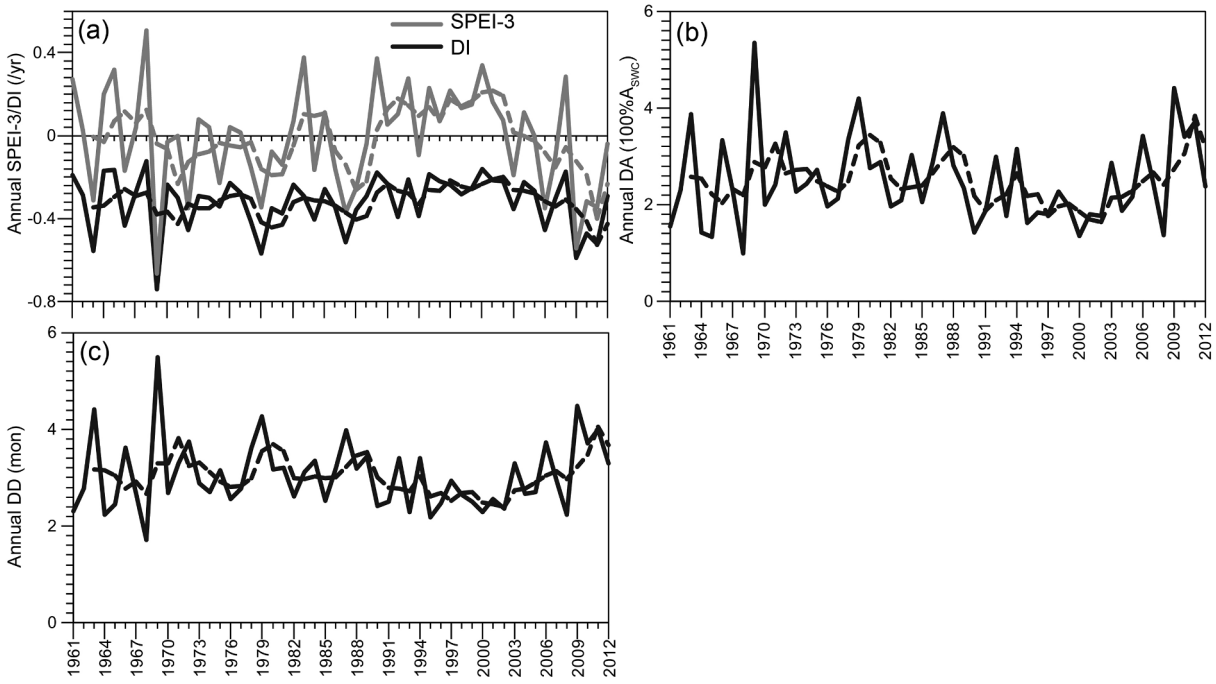

Fig. 3. Annual time series of SWC mean SPEI-3 and drought regions' mean drought parameters during 1961–2012. The dashed line represents the three-year running mean.

$^{SPEI_ET0only}SPEI_{i,k,j}$ represent SPEI-3 from $SPEI_P_{only}$ and $SPEI_ET_{0only}$ in the *j*th month of the *k*th year at the *i*th grid, respectively.

3. Results

3.1. Recent climate conditions

3.1.1. P and ET_0 anomalies during 2009–2011

During 1961–2012, the annual SWC P was mostly above normal before 2000 and then became negative afterward (Fig. 2a1). In a ranking of the 52-year P records, the 2009 and 2011P values were the second-lowest (anomalies of −142.94 mm) and lowest (anomalies of −163.52 mm), respectively, followed by the lowest three years' running mean during 2009–2011 (anomalies of −113.36 mm). The time series of the annual SWC ET_0 (Fig. 2b1) demonstrates positive anomalies before 1980 and after 2000 but negative ones between these two periods. Corresponding to the annual SWC P during 2009–2011, positive anomalies of the annual SWC ET_0 (Fig. 2b1) are found, with values of approximately 20 mm. Undoubtedly, a higher ET_0 (more water demand) and lower P (less water supply) would be likely to have exacerbated the water deficit over SWC during the preceding three years. To better understand the P and ET_0 anomalies over drought

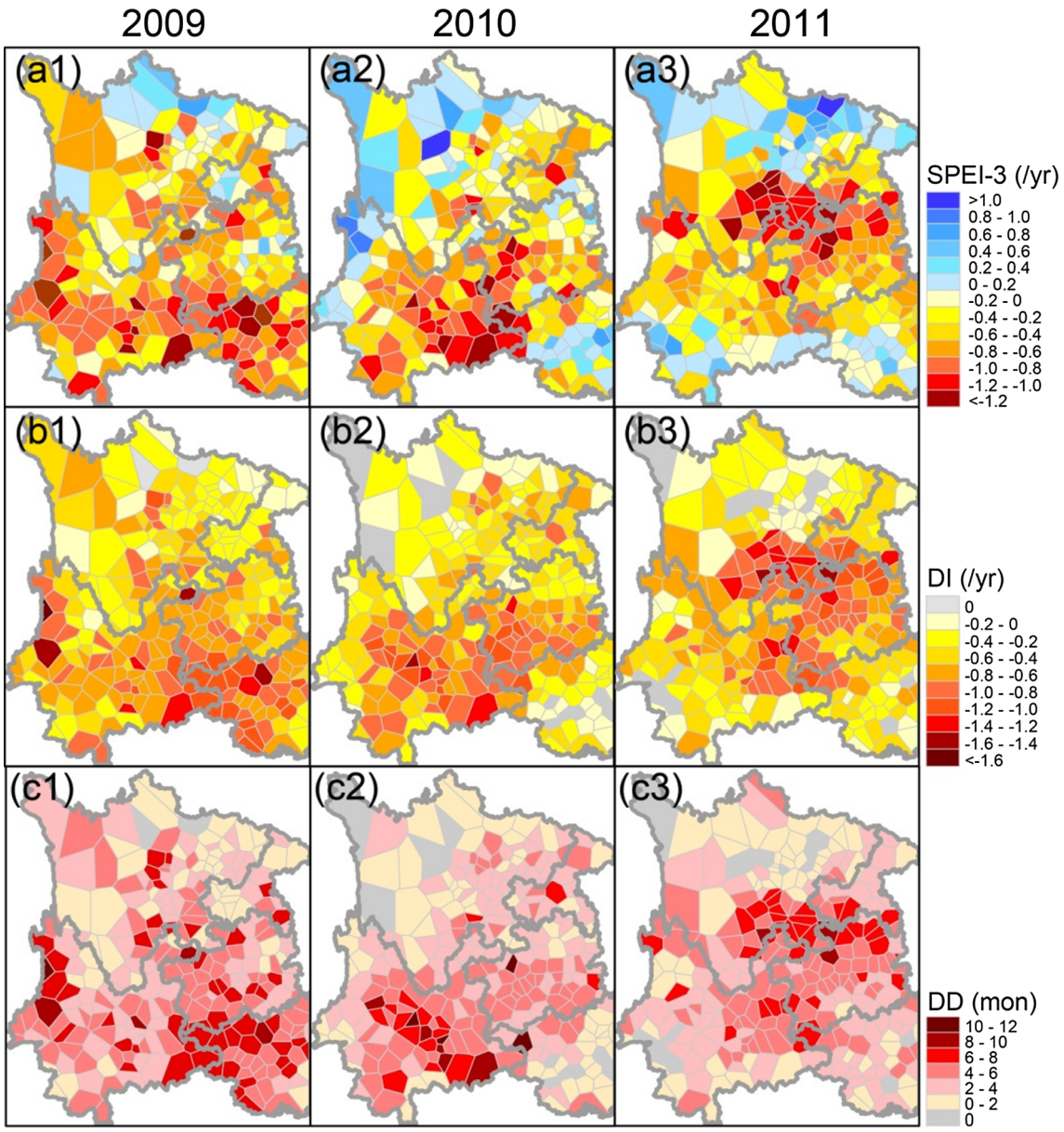

Fig. 4. Spatial distributions of the annual SPEI-3, DI, and DD during 2009–2011.

regions, we also calculated their annual values during 1961–2012 (Fig. 2a1 and b1 for P and ET_0, respectively). It is evident that SWC droughts are always accompanied by negative P and positive ET_0 anomalies. Interestingly, the P and ET_0 anomalies of SWC are closer to those of drought regions since 2005, especially for 2009–2011, which suggests that drought occurred widely and severely over SWC in this period. The intra-annual P (ET_0) anomalies over SWC and drought regions during 2009–2011 were plotted as shown in Fig. 2a2 (Fig. 2b2) to illustrate the drought evolution in those three years. Obviously, both SWC and drought regions exhibit different water deficit levels (P anomalies < 0) for most of the 36 months, especially for September–November 2009 and July–September 2011, with larger anomalies of < −20 mm (Fig. 2a2). As indicated in Fig. 2b2, there generally exists a similar intra-annual fluctuation of the ET_0 anomaly between drought regions and SWC, characterized by maxima (> 5 mm) in October–November 2009, February–March 2010, and July–October 2011. Moreover, the drought regions' ET_0 anomalies are always positive for each month, consequently intensifying the water deficit by creating more water demand. In summary, under the combined effects of negative P and positive ET_0 with higher anomaly magnitudes, there is potential for the occurrence of more severe droughts over SWC.

3.1.2. SPEI-3 and drought characteristics during 2009–2011

To examine the dry/wet conditions and drought characteristics over SWC, we calculated the annual SWC SPEI-3 and identified relevant drought parameters (DI, DA, and DD), which are shown in Fig. 3. Fig. 3a shows that SWC was generally wetter (SPEI-3 > 0) in the 1960s, 1990s–2000s, and the first half of the 2010s, but drier (SPEI-3 < 0) in other years, particularly after 2008. In broad terms, similar trends are evident for SWC DA and DD fluctuations, i.e., slight decreases since the 1990s and then sharp increases from 2000 on (Fig. 3b and c). Interestingly, in spite of the 1960s generally being wetter, the driest year in the study period was 1969, based on SPEI-3 and the three drought parameters, and the next driest year was 2009 (−0.54/yr, −0.59/yr, 441% A_{SWC}, and 4.48 mon for SPEI-3, DI, DA, and DD, respectively; Fig. 3). However, considering the three-year running means, the most severe drought in SWC was found to be in 2009–2011, characterized by the lowest DI (−0.53/yr) and the highest DA (384% A_{SWC}) and DD

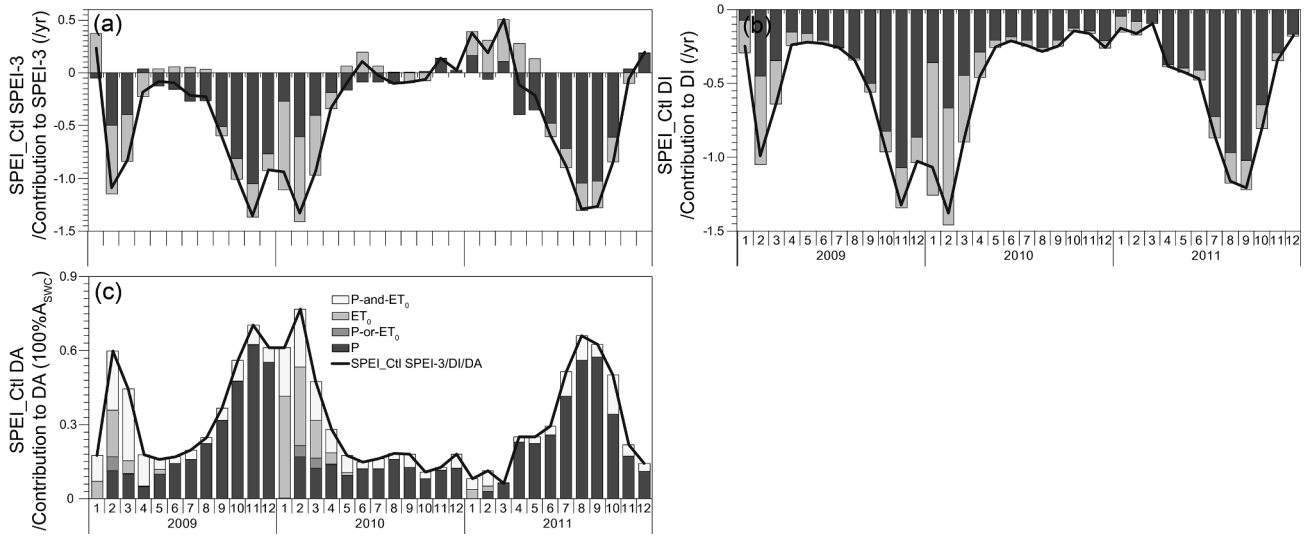

Fig. 5. Monthly evolution of the SWC SPEI-3 and drought regions' DI and DD during 2009–2011, with each driving factor's contribution.

(4.06 mon), mainly because of the lowest (higher) three-year running P (ET_0). Fig. 4 illustrates the spatial distributions of the annual SPEI-3, DI, and DD in 2009–2011. Overall, SWC was drier, excluding the mid-north of SC, in 2009; western SC, westernmost YN, and the mid-south of wGX in 2010; and the northern and southernmost parts of SWC in 2011 (Fig. 4a1–3). The driest areas (SPEI-3 < −0.8/yr) were the westernmost and southern areas of SWC in 2009, the mid-south of SWC in 2010, and southeastern SC and northern GZ in 2011. It is evident that the overwhelming majority (> 90% A_{SWC}) of SWC experienced at least once drought from 2009 to 2011 (Fig. 4b1–3 and c1–3). The annual DI (Fig. 4b1–3; DD, Fig. 4c1–3) was less (greater) than −0.6/yr (5 mon) over more than 40% A_{SWC} for these three years, mainly in southern SWC in 2009, YN (except for the westernmost part) and southern GZ in 2010, and the mid-east of SWC in 2011.

Fig. 5 illustrates the monthly evolution of the SWC SPEI-3 and the DI and DD of the drought regions during 2009–2011. Except for eight months that were slightly wetter during the three-year period (SPEI-3 < 0.5/yr; Fig. 5a), SWC was drier, especially in February–March 2009, September 2009–March 2010, and June–October 2011, with SPEI-3 < −0.5/yr. Similarly, based on the monthly drought regions' DI (< −0.5/yr) and DA (> 45% A_{SWC}), the drought was more severe in these months (Fig. 5b and c). Fig. 6 illustrates the spatial distributions of the monthly SPEI-3/DI during 2009–2011. During January and April–July of 2009, limited areas in SWC had drier conditions/drought, while larger areas suffered from drier conditions during the remaining months (Fig. 6a). In particular, more than 50% A_{SWC} was subjected to drought in February (mainly in southeastern SWC and eastern SC; Fig. 6a2) and during October–December (mainly in southern SWC; Fig. 6a10–12). In 2010, a negative SPEI-3 (drought) is widely distributed over SWC in January-May (Fig. 6b1–5) and October (Fig. 6b10), especially with drought regions covering more than 80% A_{SWC} in January and February. In contrast, most of SWC was covered by wetter conditions in the other six months (Fig. 6b6–9, b11, and b12). Fig. 6c1–3 show that more than 70% A_{SWC} was wetter during January–March of 2011, whereas nearly 90% (more than 50%) of SWC exhibited drier conditions (drought) in June–October (Fig. 6c6–10). However, comparable areas of drier and wetter conditions were presented in the remaining months (Fig. 6c4, c5, c11, and b12).

3.2. Climate anomaly impacts on drought during 2009–2011

3.2.1. Performance of the separation method

To obtain more accurate results regarding the contribution of each driving factor to the SPEI-3 anomaly, the separation method proposed by Sun et al. (2014, 2017b) was further developed and employed in this study. The cumulative contributions of each factor were calculated for comparison against monthly and annual SPEI_Ctl SPEI-3 anomalies. Fig. 7a shows the scatter-plot of the annual cumulative contributions and SPEI_Ctl SPEI-3 anomalies averaged over the entirety of SWC. Intuitively, each data point of the annual SPEI_Ctl SPEI-3 anomaly vs. cumulative contributions is closer to the 1:1 line. Combining the results for all 52 years, a fitted linear equation was derived with a regression coefficient (*Slp*) of 1.025 and an *R* of 0.999. We also calculated the annual *Slp* and *R* at each site, as shown in Fig. 7b and c, respectively. For an overwhelming majority of the 269 sites, the annual *Slp* is between 1.00 and 1.04, with $R > 0.998$. Based on these results, the annual *Slp* and *R* quantitatively indicate that this method can accurately identify each driving factor's contribution to annual SPEI-3 anomalies on regional and site-based scales for the time period of 1961–2012. To further examine the robustness of this approach, monthly results were also compared (Fig. S1–3). For each month, all data points of the monthly SPEI_Ctl SPEI-3 anomaly vs. cumulative contributions are very close to the 1:1 line (Fig. S1), with *Slp* and *R* values ranging from 1.001 to 1.196 and from 0.997 to 0.999, respectively. For each site (Figs. S2 and S3), *Slp* (*R*) is always between 0.96 and 1.04 (> 0.998) for every month except January and February, suggesting that the method as improved in this study also achieves better separation of each factor's contribution to the monthly SPEI-3 anomalies. As a result, this improved method, with higher accuracy and efficiency, proved to be a useful tool for quantifying the contribution of climate anomalies to SPEI-3 and drought indicators (i.e., DI, DD, and DA) in this study.

3.2.2. Contributions to DI

Fig. 8 shows the P and ET_0 anomalies' contributions to the annual drought regions' DI during 2009–2011. Overall, DI was strengthened in response to decreased P (increased ET_0) in those three years, with a P (ET_0) contribution of −0.44/yr (−0.16/yr) in 2009, −0.28/yr (−0.22/yr) in 2010, and −0.44/yr (−0.09/yr) in 2011. Therefore, the DI in each year can be attributed to a negative P. However, it should be noted that P and ET_0 exerted comparable impacts on DI in 2010. To understand the spatial distributions of the P and ET_0 contributions to the annual DI in each year, their impacts were estimated at each Thiessen grid (Fig. 9). In general, drought occurrence is accompanied by negative contributions of P and ET_0 over the whole region. In 2009, the P contribution ranged from −1.31 to 0/yr and was generally smaller in SC and CQ and larger in other regions, especially at the junction of YN, GZ, and wGX (< −0.7/yr; Fig. 9a1). For the ET_0 contribution, the magnitude was generally lower than 0.5/yr, with regions

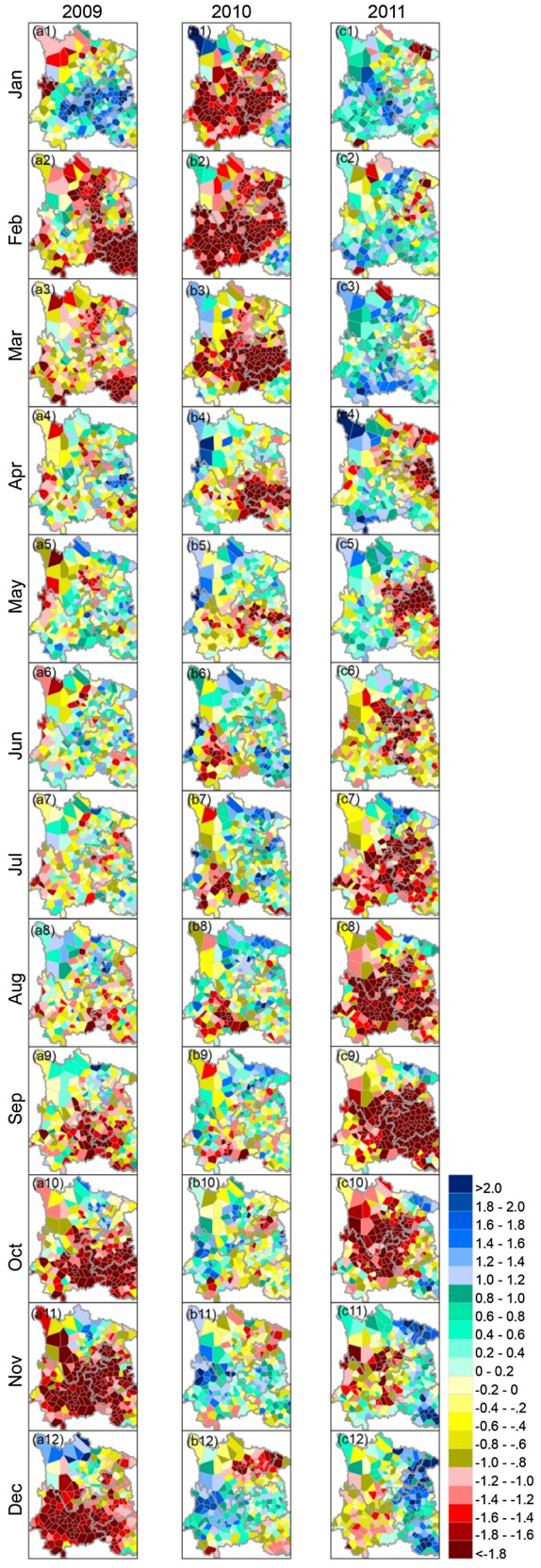

Fig. 6. Spatial distributions of the monthly SPEI-3/DI during 2009–2012. The red legend (from pale to dark red) is for DI.

of larger values (> 0.2/yr) in northwestern SC and YN and western wGX (Fig. 9a2). During 2010, except for western SC and southern wGX, a larger P contribution (< −0.2/yr) was widely distributed over the remaining regions, particularly in southern GZ and central YN (< −0.4/yr; Fig. 9a2). There was a smaller ET_0 contribution (> −0.2/yr) in most of SC and wGX and in northeastern GZ; however, the ET_0 contribution was lower than −0.2/yr in the other regions and even exceeded −0.5/yr at the junction of YN, GZ, and wGX (Fig. 9b2). The P contribution during 2011 was lower than −0.6/yr in nearly half of SWC, mainly in southern SC, mid-eastern YN, and GZ (excluding the southern part; Fig. 9a3). It is evident that, except at the junction of YN, SC, GZ, and CQ, the ET_0 contribution in an overwhelming majority of SWC was higher than −0.2/yr (Fig. 9b3). By comparing the P and ET_0 contributions, we identified the determinants (i.e., P and ET_0) of DI at the Thiessen grids (Fig. 9c1–3). The determinant of P to DI was extensively distributed over SWC from 2009 to 2011, corresponding to area percentages of 83.83% A_{SWC}, 56.27% A_{SWC}, and 86.54% A_{SWC}, respectively. Additionally, the determinant of ET_0 was mainly located in northwestern SWC in 2009; western SC, northwestern YN, and the junction of YN, GZ, and wGX in 2010; and mid-western SC in 2011.

Fig. 5b depicts the intra-annual DI evolution for all the drought regions with the monthly contributions of P and ET_0. In January–March of 2009 and 2010, the increased ET_0 had a larger contribution to DI than did the decreased P, suggesting that ET_0 was the determinant; however, DI can be attributed to a P reduction from April to December because of the much larger contribution of P. For 2011, except in January and February when ET_0 dominated, decreased P was the major contributor of DI in the remaining months. At each Thiessen grid within the drought regions, the monthly contributions of P and ET_0 to DI were estimated, and the dominants were thus identified (Fig. S4 and Table 2). By comparing the area percentages of P and ET_0 as determinants in each month (Table 2), the dominant of ET_0 was found to occupy nearly the entirety of the drought regions in January of 2009–2011, corresponding to the locations in northwestern SC (Fig. S4g1), most of SWC (except for northern and mid-western SC, and most of wGX; Fig. S4h1), and the junction of SC and CQ (Fig. S4i1), respectively. In February, the determinant of ET_0 for the three years had a larger area percentage, which generally was manifested in SC and GZ drought regions in 2009 (Fig. S4g2); western SC and GZ, YN, and northwestern wGX in 2010 (Fig. S4h2); and mid-northern SC in 2011 (Fig. S4i2). Except in March of 2011 (Fig. S4i3), there was a comparable (larger) area percentage of the determinant of ET_0 in 2009 (Fig. S4g3; 2010, Fig. S4h3), which mainly appeared in northwestern SC and GZ and mid-northern wGX (mid-western SWC). For each of the remaining months, the area percentage of the P determinant far outweighed that of ET_0 (Figs. S4g4–12, S4h4–12, and S4i4–12).

3.2.3. Contributions to DA and DD

Fig. 8b depicts the contributions of P, ET_0, P-or-ET_0, and P-and-ET_0 to the annual total DA during 2009–2011. In 2009 and 2011, the P contribution to DA was approximately 290% A_{SWC}, followed by P-and-ET_0, with contributions of < 120% A_{SWC}; moreover, the ET_0 and P-or-ET_0 contributions to DA were much smaller (< 33% A_{SWC}), especially for 2011, with percentages of 5.8% and 0%, respectively. In contrast, the P, ET_0, and P-and-ET_0 contributions in 2010 were comparable (approximately 100% A_{SWC}). In January and February of 2009 (Fig. 5c), the maximum contribution (> 10% A_{SWC}) to monthly DA was from P-and-ET_0, followed by the ET_0 contribution of more than 7% A_{SWC}. In March, P-and-ET_0 contributed to 28.9% A_{SWC}, while approximately 10% A_{SWC} was determined by P. During April, 4.9% A_{SWC} and 12.6% A_{SWC} were controlled by P and P-and-ET_0, respectively. For each month during May–December, P corresponded to the largest area percentages,

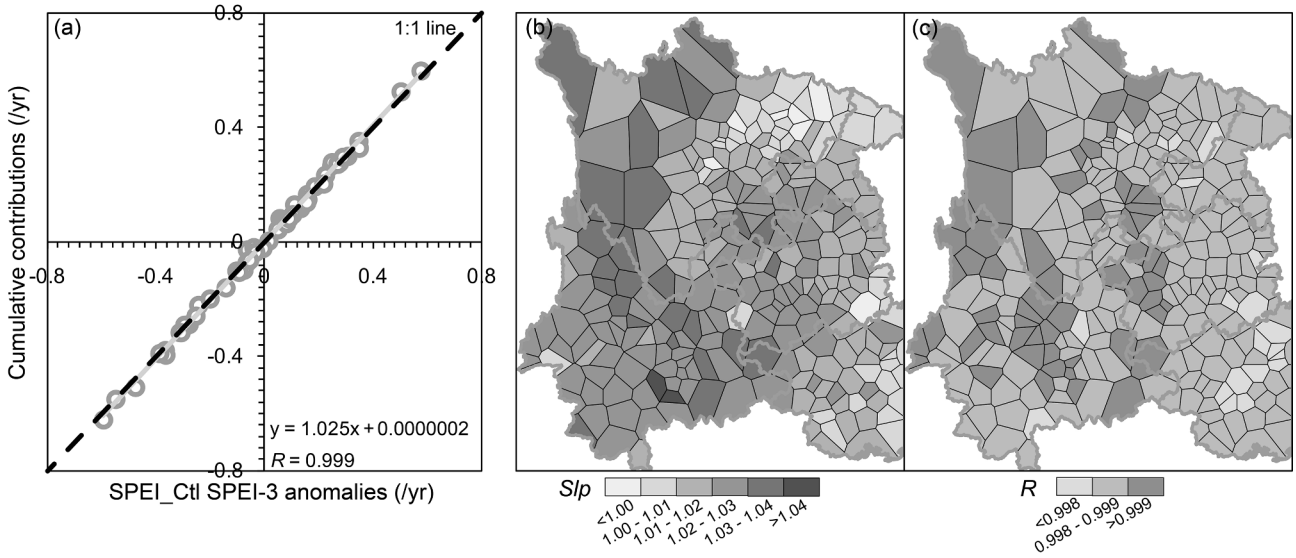

Fig. 7. Performance of the selected separation method at the annual scale. (a) Scatterplot of the SWC annual SPEI-3 anomalies from SPEI_Ctl against cumulative contributions from each climate variable during 1961–2012. (b) Spatial distribution of the regression coefficients (named as *Slp*), which can be derived from the equation: annual SPEI_Ctl SPEI-3 anomaly = annual cumulative contributions × *Slp* + constant. (c) *R* is the correlation coefficient between the annual cumulative contributions and the annual SPEI_Ctl SPEI-3 anomaly during 1961–2012.

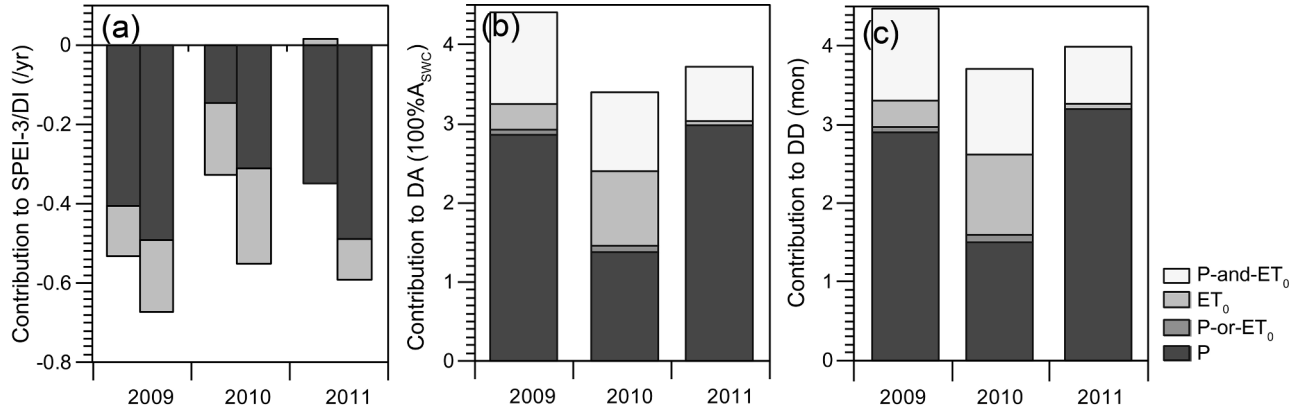

Fig. 8. Annual contributions of each driving factor to SWC SPEI-3, and drought regions' DI, DA, and DD during 2009–2011. In (a), the left of a paired bar is for SPEI-3, but the right one is for DI.

with a range of 9.9% to 62.3% A_{SWC}. During January–February of 2010, the major contributor to monthly DA was ET_0, with contributions greater than 31%, and P-and-ET_0 played a secondary role, with contributions of approximately 20%. In March, the contributions of P-and-ET_0, ET_0, and P were comparable (approximately 15% A_{SWC}). In April, 13.8% A_{SWC} was dominated by P, and less thna 4% A_{SWC} corresponded to the ET_0 or the P-and-ET_0 dominants. A comparable area percentage (< 10% A_{SWC}) from P-and-ET_0 and P was detected for May. During June–December, DA could always be attributed to P-and-ET_0 and P, with P having a larger contribution (8% to 16% A_{SWC}). In January and February of 2011, P-and-ET_0 was the major contributor, while in the remaining months, P generally governed all the drought regions, with an area percentage between 6.1% A_{SWC} in March and 57.5% A_{SWC} in September. Spatial distributions of the dominants of the monthly DA during 2009–2011 are depicted in Fig. S5. Briefly, the spatial distributions of the dominants differ from month to month. Details of the analyses can be found in Text S2.

As with the contributors to DA, P reduction was probably responsible for the annual SWC DD during 2009–2011, with contributions of 2.90 mon, 1.50 mon, and 3.20 mon, respectively (Fig. 8c). P-and-ET_0 in 2009 and P-and-ET_0 and ET_0 in 2010 were > 1.00 mon and played secondary roles in the annual SWC DD, while the impacts of ET_0 (not including ET_0 in 2010) and P-or-ET_0 in 2009–2011 were very limited, particularly for P-or-ET_0, with contributions less than 0.10 mon. For all Thiessen grids, we calculated the P, ET_0, P-or-ET_0, and P-and-ET_0 contributions to the annual DD from 2009 to 2011 (Fig. 10). In 2009 (Fig. 10a1), the determinant of P with contributions ≥1 mon to the annual DD was widely distributed over the drought regions; moreover, its contribution was ≥4 mon in most of southern SWC, especially at the junction of YN, GZ, and wGX (≥5 mon). As seen from their contributions (≤4 mon) and spatial extents (Fig. 10a2–3), ET_0 or P-or-ET_0 were dominant only in certain months and regions. While most grids had a determinant of P-and-ET_0 (Fig. 10a4), its contribution was ≤3 mon, except for several grids in mid-western YN (≥5 mon). In 2010 (Fig. 10b1, b2, and b4), P, ET_0, or P-and-ET_0 had extensive spatial extents (> 50% A_{SWC}) as determinants for annual DD, but their contributions generally ranged from 1 to 4 mon. As shown in Fig. 10b2, a very limited spatial extent generally corresponds to a P-or-ET_0 dominant with a contribution between 1 and 2 mon. Compared to each factor's contribution to the annual DD and spatial extent in 2011 (Fig. 10c1–4), there were larger regions with P contributions ≥4 mon in the middle of SWC, suggesting that drought occurrences in most of the months of 2011 were closely associated with P. Despite there having been a greater spatial extent for the dominant of P-and-ET_0, its

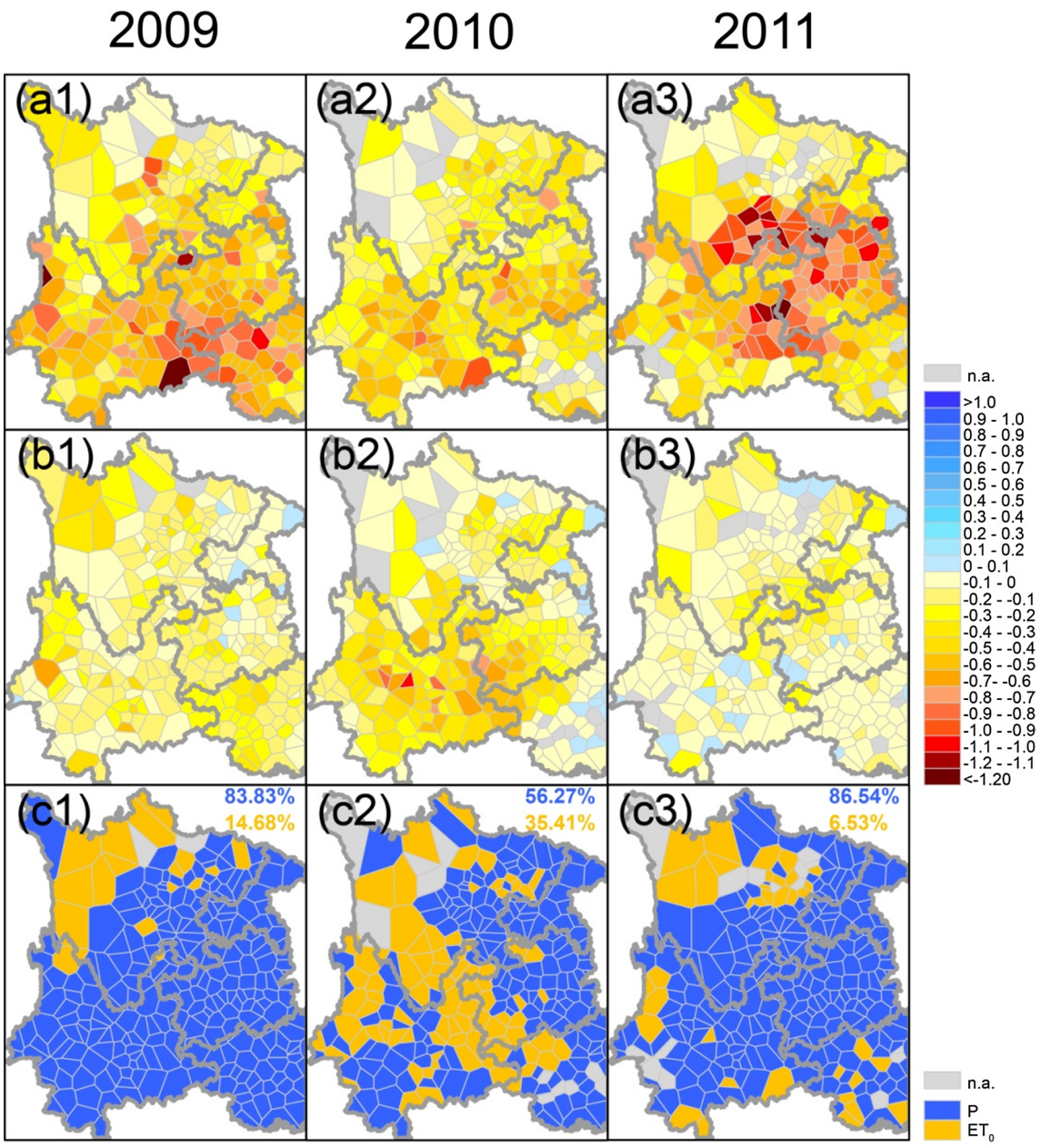

Fig. 9. Spatial distributions of climate anomalies' impacts on the annual DI and determinants during 2009–2011. (a) and (b) are the P and ET_0 contributions, respectively, while (c) denotes determinants of P or ET_0. In (c), blue and yellow numbers indicate the area percentage of the determinant of P or ET_0, respectively.

Table 2
Area percentage ($\%A_{SWC}$) for the determinants of DI during 2009–2011.

Determinant	2009		2010		2011	
	P	ET_0	P	ET_0	P	ET_0
Annual	83.83	14.68	56.27	35.41	86.54	6.5
Jan	1.21	16.21	3.3	58.01	0.54	7.66
Feb	24.33	35.42	30.22	46.58	3.72	7.71
Mar	27.59	16.77	21.97	25.41	6.34	0
Apr	13.98	3.72	18.45	9.68	25.15	0
May	11.54	4.38	14.19	3.22	23.83	1.2
Jun	17.04	0	14.50	0.45	29.36	0
Jul	18.93	0.78	16.12	0	49.99	1.47
Aug	23.94	0.78	18.37	0	65.35	0.68
Sep	36.73	0	18.09	0	62.31	0.19
Oct	56.02	0	10.69	0	49.94	0.18
Nov	70.36	0	12.55	0	21.77	0
Dec	60.03	0	17.57	0.46	14.23	0.15

contribution was generally ≤2 mon, which suggests that this factor was critical for drought occurrences in several months (Fig. 10c4). In addition, it is very evident that the role of ET_0 or P-or-ET_0 in the 2011 drought occurrences was very limited, given the contributions of ≤1 mon in several grids.

4. Discussion

4.1. Circulation patterns associated with negative P anomalies over SWC during 2009–2011

As discussed above, negative P anomalies occurred over SWC from 2009 to 2011, with the 2009 and 2011P anomalies ranking in the top two events during 1961–2012. Additionally, negative P anomalies were more obvious during August–November 2009 (Fig. 2a2 and Fig. 11a) and July–October 2011 (Fig. 2a2 and Fig. 11b). As a result, we chose to focus on these months to briefly examine the possible causes of negative

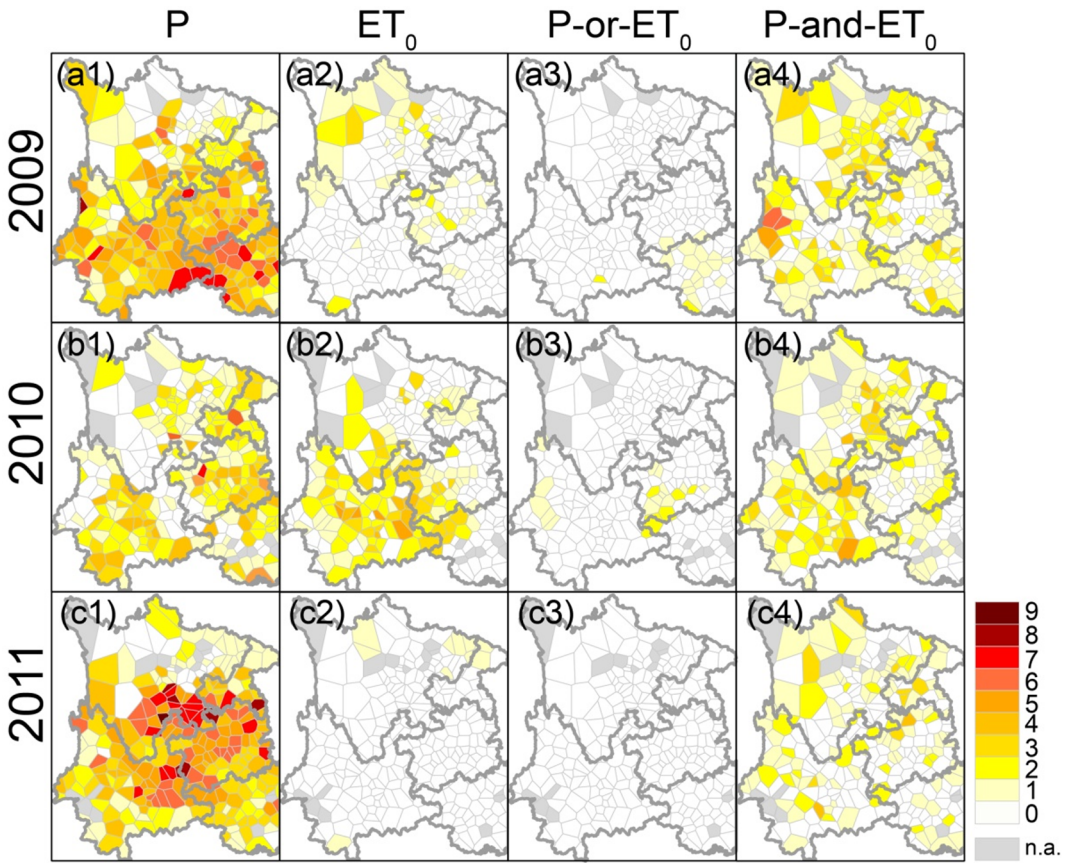

Fig. 10. Spatial distributions of climate anomalies' impacts on annual DD.

P anomalies from atmospheric circulation patterns (Fig. 11c and d). Fig. 11a shows that negative P anomalies were larger in the middle and southern parts of SWC during August–November 2009, coincident with concurrent greater DI (Fig. 6a8–11). The column-integrated water vapor flux indicates a strong cyclonic anomaly over the tropical west Pacific, with strengthened southwestward water vapor flux anomalies in the middle and southern portions of SWC during August–November 2009 (Fig. 11c). The warm tropical Northwest Pacific sea surface temperature related to El Niño has been proposed as a forcing for this cyclonic anomaly (Zhang et al., 2013a,b; Wang et al., 2015a,b), thereby weakening the transport of moisture from the Northwest Pacific into SWC. On the other hand, although a weak cyclonic anomaly is located in the east of the Bay of Bengal (Fig. 11c), its poleward water vapor flux anomalies are suppressed, in contrast to the reinforced westerly anomalies in the vicinity of the equatorial Indian Ocean due to the warm tropical Northwest Pacific sea surface temperature (Wang et al., 2015a,b). As a result, anomalous water vapor flux divergence dominated the middle and south of SWC during August–November 2009 (Fig. 11c). As seen from Fig. 11d, the SWC circulation patterns during July–October 2011 were, to some degree, akin to those during August–November 2009. That is, enhanced northeasterly water vapor flux anomalies associated with an anomalous tropical western Pacific low prevailed in the eastern and southern portions of SWC; southerly water vapor flux anomalies with respect to the weak cyclonic anomaly centered in the east Bay of Bengal are obviously relaxed (Fig. 11d). Therefore, anomalous water vapor flux divergence is predominant in those regions (Fig. 11d) and reduces P.

Notably, the spatial patterns of P anomalies are not strictly consistent with those of anomalous water vapor flux and divergence. This implies that, in addition to the possible causes of moisture transport and atmospheric dynamic anomalies, which are closely related to sea surface temperature and the atmosphere's internal variability, other forcings (e.g., greenhouse gases, aerosols, solar activities, and topography) should also be more or less responsible for anomalous P. These factors can directly or indirectly impact P processes via a series of complex physical processes and mechanisms (Bollasina et al., 2011; Marvel and Bonfils, 2013; Liao et al., 2015; Sarojini et al., 2016; Ning et al., 2017; Zhao et al., 2017). For example, greenhouse gases induce global warming and thereby change the hydrological cycle, including P (Liu et al., 2015a, b, c; Shi et al., 2015). Through aerosol–radiation (direct effect) and aerosol–cloud interactions (indirect effect), aerosols can contribute to P variations (Liao et al., 2015) and even exert greater impacts on P than do greenhouse gases (Bollasina et al., 2011). As one of the major sources of energy for forcing the climate system, any solar variations (e.g., an 11-year solar cycle) will be more or less reflected in P (van Loon and Meehl, 2012; Kodera and Shibata, 2006; Chen et al., 2015a; Zhao et al., 2017). P is strongly impacted by topography (more complex terrain over SWC in Fig. 1; e.g., Liu et al., 2015b, c), local evapotranspiration (e.g.Huang and Cui, 2015; Wei et al., 2015; Li et al., 2016; Zhang et al., 2017b), and land use/cover change (e.g., urbanization (Chen et al., 2015b) and deforestation (Devaraju et al., 2015)). It should be noted that these influential factors, including the natural internal variability of the climate system, external forcings, and others, are not independent but may often be mutually connected through atmospheric circulation and complex physical processes and mechanisms. The potential causes of P anomalies are extremely complex; therefore, to further explore the related explanations, we need to quantitatively and comprehensively consider these driving factors and their linkages in future research.

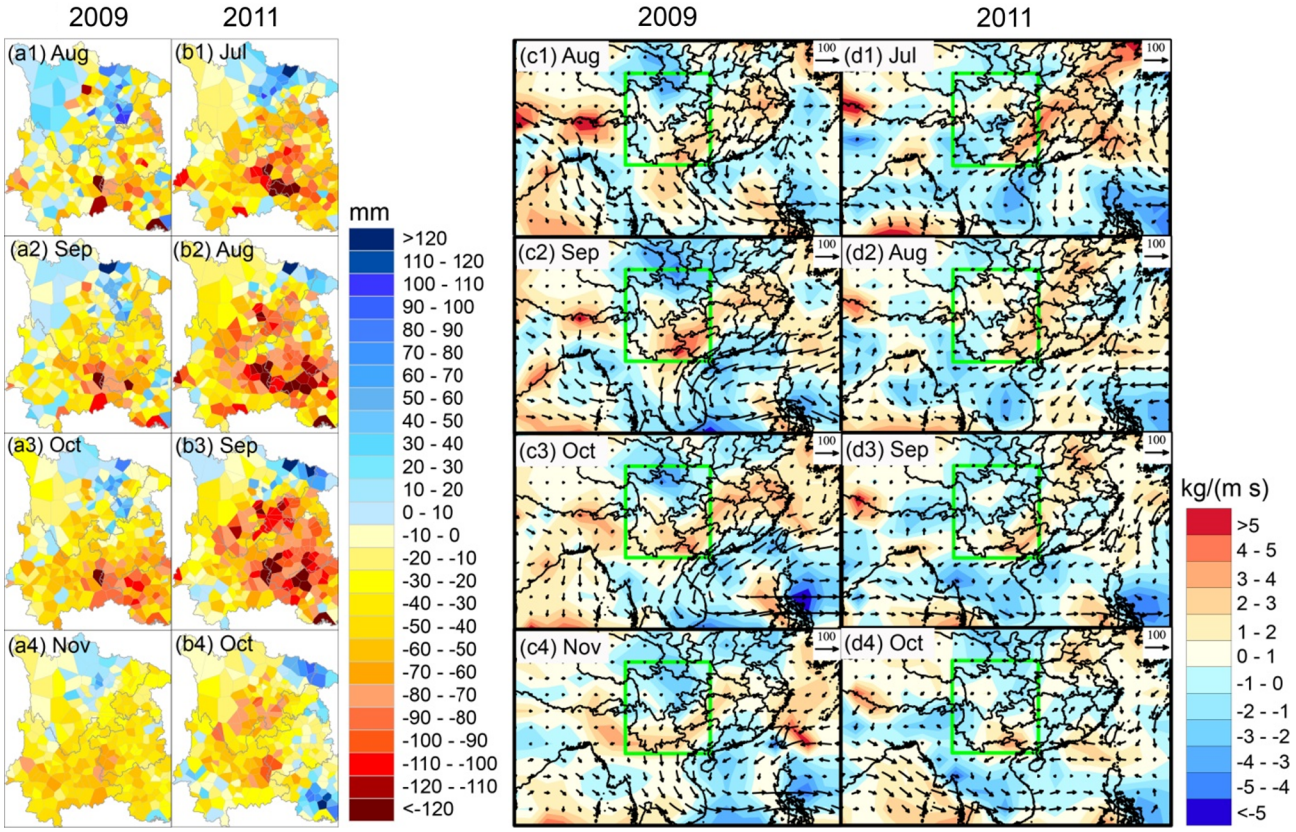

Fig. 11. Monthly anomalous P for August–November 2009 (a1–4) and July–October 2011 (b1–4) and its corresponding column-integrated water vapor flux over a depth from the surface to 300 hPa [kg/(m s); c1–4] and divergence [10^{-5} kg/(m^2 s); d1–4]. In (c) and (d), the shaded area and the vector represent column-integrated water vapor flux and divergence, respectively, and the location of SWC is specified by the green rectangle.

4.2. Attribution of positive ET_0 anomalies over drought regions during 2009–2011

Despite numerous analyses of long-term changes (i.e., linear trends; Sun et al., 2017b) in ET_0 in SWC, the changes in the magnitude of ET_0 in the context of droughts and which climate variables control ET_0 variations have scarcely been investigated to date. As noted above, we found that both the annual and monthly ET_0 values averaged over drought regions increase by different rates, thereby intensifying the drought to some extent. Therefore, we identified ET_0 changes over drought regions, which should be helpful in understanding drought evolutions well. Fig. 12a suggests that changes in each driving factor (i.e., increased *SSD*, *Tave*, and U_2 and decreased *Rh*; not shown here) generally increased the annual ET_0 over drought regions during the study period. However, each factor's contribution differed from year to year; thus, the dominant factor (with the largest contribution) of positive ET_0 anomalies exhibited inter-annual variations, i.e., negative *Rh*, positive *U2*, negative *Rh*, and positive *Tave* and negative *Rh* anomalies contributing primarily in the 1960s, 1970 s, 1980s, and 1991–2012, respectively. Moreover, the contributions of *Rh* and *Tave* were both greater than 10 mm during 2009–2012, which suggests that these two factors play critical roles in the positive anomalies of annual ET_0. As depicted in Fig. 12b, each factor had an essentially positive contribution to the monthly drought regions' ET_0, except for U_2, which had smaller (> 0.3 mm) negative contributions in several months (e.g., June and July 2009, February and May 2010, and April 2011). A comparison of the contributions of each factor shows that the increased *Tave* should be responsible for the positive ET_0 anomalies in January–November 2009 (11 mon), February and June–November 2010 (7 mon), and June–August and October 2011 (4 mon), while other months have the determinant of decreased *Rh*.

It is apparent that at the overwhelming majority of grids (> 90% A_{SWC}), the annual ET_0 in the three selected years increased to different degrees, i.e., the larger values (> 40 mm) occurred mainly in western wGX and the junction of YN and GZ in 2009 (Fig. 13a1); throughout YN (excluding the west part), northwestern wGX, and southwestern GZ in 2010 (Fig. 13a2); and at the junction of YN, SC, CQ, and GZ and in northern wGX in 2011 (Fig. 13a3). In the context of drought, the annual ET_0 generally increased due to increased *SSD* for most grids during 2009–2011 (Fig. 13b1–3), especially for 2011, with an area percentage of more than 90% A_{SWC}; however, the contributions were all smaller than 30 mm. As seen in Fig. 13c1–3 (Fig. 13d1–3), more than 90 nomalies. Notably, there were similar spatial distributions of *Tave* and *Rh* contributions, followed by a center of higher values (> 20 mm), in most of wGX in 2009, YN (excluding the western parts) in 2010, and at the junction of SC, YN, and CQ in 2011. The U_2 contribution in each year (Fig. 13e1–3) is spatially complex, generally being characterized by nearly 50% A_{SWC} with positive impacts. Table 3 illustrates that, on an annual scale, more than 80% A_{SWC} had the major contributors of *Tave* and *Rh*. The area percentage of the *Tave* determinant (70.88% A_{SWC}) was much larger than that of the *Rh* determinant (17.57% A_{SWC}) in 2009, but the area percentages of these two factors were comparable (approximately 40% A_{SWC}). Despite all of that, their distributions differed from year to year. In 2009, the *Tave* determinant was widely distributed over SWC, except in mid-western SC, northwestern GZ, some parts of YN, and southwestern wGX, with the *Rh* determinant (Fig. 13f1). In 2010, the *Tave* determinant was mainly located in northern SWC (excluding mid-western SC) and southwestern YN (Fig. 13f2). In 2011, western SWC, southern CQ, and western GZ basically had the *Tave* determinant (Fig. 13f3). As Table 3 shows, except in a few months (i.e., July and August 2009 and December 2011), the monthly ET_0 anomalies over most of the drought regions could be

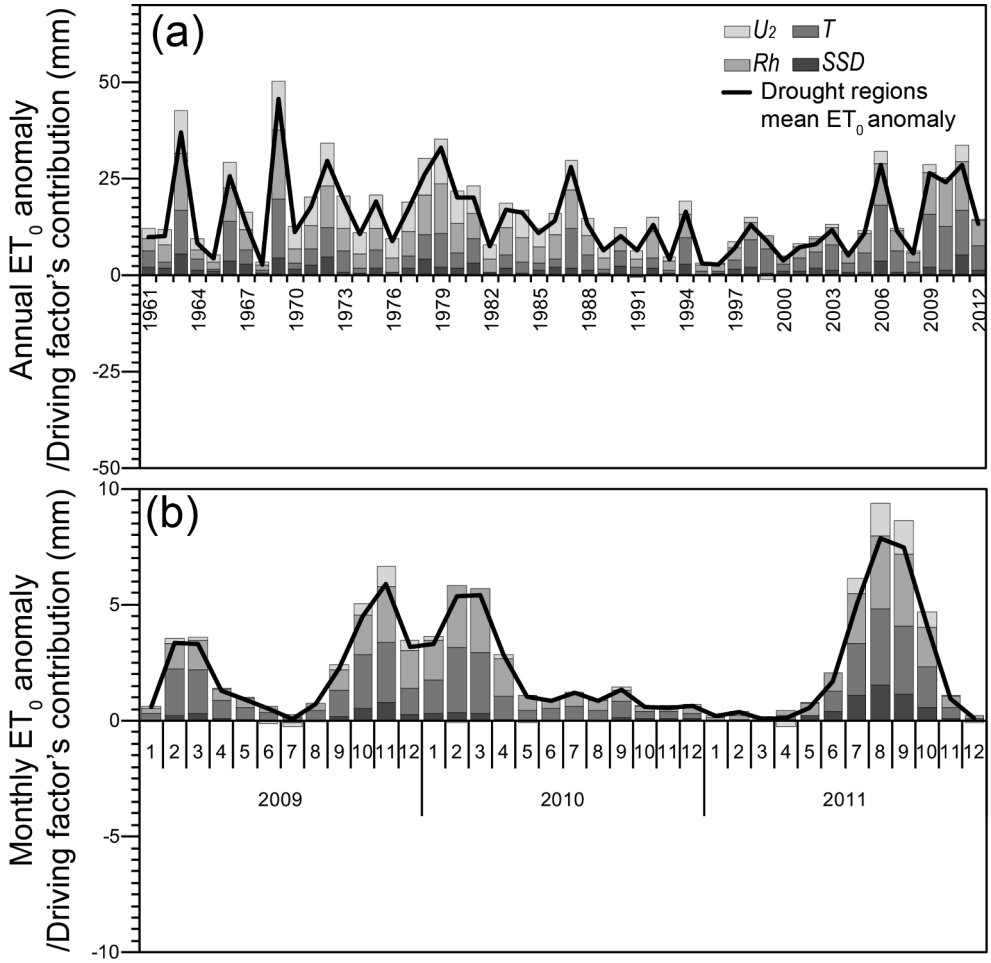

Fig. 12. Contributions from the major driving factors to the annual and monthly ET_0 anomalies during 2009–2011.

attributed to *Tave* or *Rh* for the period of 2009–2011. Essentially, the anomalously higher *Tave* or lower *Rh* should be responsible for the positive ET_0 anomalies over the drought regions on different spatial (i.e., the entire SWC and Thiessen grid) and temporal (i.e., annual and monthly) scales, while the *SSD* and U_2 contributions are much more limited.

4.3. Uncertainties

There exist some uncertainties in this study, mainly because of the constant albedo of the land surface (=0.23 here), elevated CO_2, soil properties, vegetation–drought interaction, etc. Because of the limited availability of solar radiation measurements in SWC, SSD was selected to estimate *Rn* at the 269 sites using the semi-physical formulas proposed by Allen et al. (1998; shown in Supplementary Text S1). In these equations, an important parameter of land surface albedo is fixed at 0.23, but in practice, this parameter exhibits evident spatiotemporal variations with climate conditions, soil moisture, and land use/cover (Liang et al., 1998; Zhang et al., 2012; Mira et al., 2015). As a result, the assumption of constant albedo may introduces uncertainties into the calculated *Rn* and even into ET_0, potentially biasing SPEI-3. Based on assumptions of a single-leaf stomatal resistance of 100 s/m under well-watered conditions, a sunlit leaf area index (LAI) of 1.44 m^2/m^2, and a surface resistance of 70 s/m (Allen et al., 1998), the FAO-56 Penman–Monteith equation was developed from the original Penman–Monteith form. Nevertheless, numerous pieces of evidence from observations and numerical simulations have proven that plant physiology responds directly to increasing CO_2 levels through changes in stomatal resistance and LAI (Feller, 2016; Gray and Brady, 2016; Xu et al., 2016; Paschalis et al., 2017). Thus, there is no doubt that the confidence levels of our results will be impacted by the effects of elevated CO_2 on vegetation that are not considered by the FAO-56 Penman–Monteith In a recent study using drought metrics with ET_0 estimates from several variants of the Penman–Monteith equation, Milly and Dunne (2016) noted that continental drying might be exaggerated, largely because of neglect of the bulk stomatal conductance response to enhanced CO_2 levels within the Penman–Monteith variants. A closer relationship exists between soil moisture (which can reflect drought) and soil types/properties, which play important roles in controlling the duration and quantity of water storage in soil layers. Park et al. (2004) reported that differences in the water-holding capacity of soil types could explain most spatial variations in soil moisture, implying that soil types/properties should be integrated into various drought metrics to more accurately characterize drought characteristics. Vegetation and droughts can interact in a very complex way. For instance, drought appears to be accompanied by decreased precipitation that leads to lower soil moisture and subsequently influences vegetation by controlling stomatal conductance and LAI (Feller, 2016; Gray and Brady,

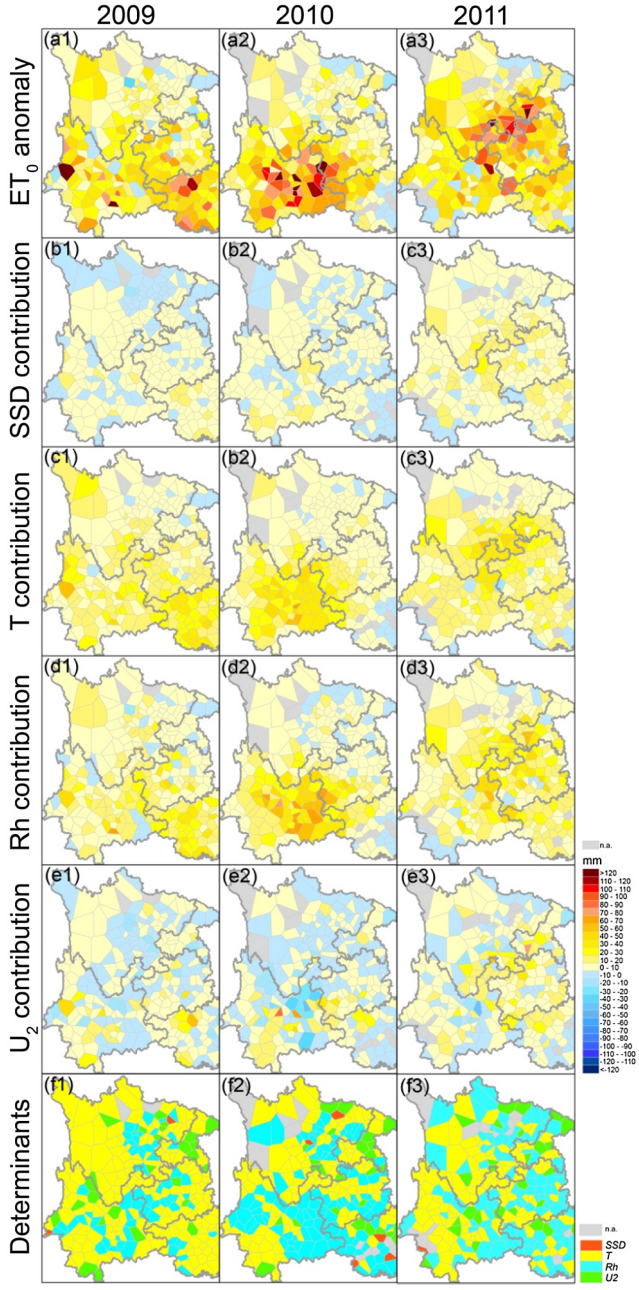

Fig. 13. Spatial distributions of the annual ET_0 anomaly, the driving factor's contribution, and the determinants during 2009–2011.

2016). Feller (2016) noted that in drought conditions, plant stomata were less open or epicuticular waxes were produced and leaf transpiration therefore decreased. Furthermore, droughts, particularly more severe droughts, usually induce a higher vapor pressure gradient between leaves and the atmosphere, leading to stress on the plant hydraulic system (Reichstein et al., 2013; Meir et al., 2015), embolism and partial failure of hydraulic transport in the stem, and even the potential for vegetation mortality (Allen et al., 2010; Scott et al., 2010; Duan et al., 2013; Gea-Izquierdo et al., 2014). Conversely, precipitation received by the land surface, ET, and soil moisture losses are significantly impacted by drought-induced vegetation changes or mortality, varying drought evolutions (Teuling et al., 2010).

In addition, several limitations of this study should be kept in mind. One widely used drought index on a three-month scale (i.e., SPEI-3), coupled with only the FAO-56 Penman-Monteith equation, was employed in this study, and this approach may potentially influence the universality of our findings, e.g., whether the roles of P and ET_0 in drought evolutions are consistent among different drought indices, on various time scales, and for a specific drought index with different potential evapotranspiration formulations. Considering the complex associations of drought with P and ET_0, expressing their separate contributions by means of linear equations [i.e., Eq. (3)] may have introduced some uncertainties into our results, despite the better performance achieved in quantifying the impacts of P and ET_0 on SPEI-3 anomalies. Thus, ignoring the influences of the aforementioned factors may have introduced some degree of uncertainty in the results of the present study. However, the mechanisms and magnitudes of these incomplete considerations that may influence drought evolutions remain unclear because of the complicated linkages among them. Therefore, more effort should be devoted to this issue in future work to achieve a more comprehensive understanding of drought mechanisms.

5. Conclusions

In this study, we utilized the 2009–2011 droughts as an example to investigate P, ET_0, and drought evolution. Over drought regions, the annual and monthly P (ET_0) during 2009–2011 were always lower (higher) than the climatological values, which probably triggered a water deficit and allowed it to persist through the decreasing water supply (increasing water demand). Under the combined effects of larger negative P and positive ET_0 anomalies in each study year, an overwhelming majority of SWC experienced at least once drought, and the annual DI (DD) was lower (greater) than -0.6/yr (5 mon) over more than 40% A_{SWC}. Moreover, the 2009 drought was the second most severe of the 1961–2012 period, based on the selected drought parameters. On a monthly scale, the drought evolution obviously varied from year to year, e.g., the drought severity was stronger in February–March 2009, September 2009–March 2010, and June–October 2011. To better understand the roles of the P and ET_0 anomalies in influencing drought evolution, we separated their individual contributions to DI, DA, and DD. For the mean for all of the drought regions, the main contributor to annual DI (DA) was P during 2009 and 2011, followed by ET_0 (ET_0 or P-and-ET_0). Furthermore, DD could be attributed to P reduction in each of the three years. At the Thiessen grid scale, in spite of most grids having determinants of P, some grids still had ET_0 (ET_0 or P-and-ET_0) as the major contributor to annual DI (DD). On a monthly scale, DI (DA) in January–March can generally be attributed to ET_0 (ET_0 or P-and-ET_0) for the three years, while the other months had a dominant P.

Based on a full analysis of the P and ET_0 contributions to drought parameters, the drought occurrence and persistence during 2009–2011 can generally be attributed to P reduction over SWC. However, the ET_0 impacts were comparable to those of P and even larger in certain regions and periods. These findings suggest that ET_0 is critical in spatiotemporal drought evolutions and even plays a determinant role. In summary, detailed analyses such as those conducted in this study facilitate a better understanding of the ongoing and intensifying droughts in SWC. Quantitative information (e.g., spatiotemporal differences in drought dominants) can be used to improve drought monitoring and forecasting systems. More importantly, the results of our study provide an important reference framework for understanding droughts and their underlying mechanisms throughout other regions of the globe, especially those with intensifying droughts.

Table 3
Area percentage (%A_{SWC}) for the determinants of ET_0 anomalies during 2009–2011 over drought regions.

Determinant	2009				2010				2011			
	SSD	*Tave*	*Rh*	U_2	*SSD*	*Tave*	*Rh*	U_2	*SSD*	*Tave*	*Rh*	U_2
Annual	0.34	70.88	17.57	9.71	2.40	43.20	37.28	8.46	0.61	42.15	40.72	9.59
Jan	0.37	10.64	4.63	1.79	0	17.12	36.73	7.46	0.55	1.16	4.34	2.15
Feb	0	50.60	5.85	3.30	0	41.95	32.78	1.98	0	0.24	7.00	4.20
Mar	0	37.40	4.84	2.12	0	21.77	23.72	1.89	0	0.67	5.00	0.68
Apr	0	15.58	0.79	1.33	0	2.80	22.61	2.72	0.29	7.69	10.75	6.42
May	0.30	8.86	3.04	3.71	0	8.31	6.22	2.88	0.47	9.12	11.85	3.60
Jun	0	13.37	3.67	0	0	13.35	1.60	0	0	16.84	12.52	0
Jul	2.55	3.66	5.13	8.37	0.49	9.72	4.49	1.43	0	28.35	18.47	4.64
Aug	3.46	4.96	4.96	11.35	1.04	8.17	7.02	2.14	0	36.77	27.34	1.91
Sep	0.98	19.71	9.86	6.18	0.20	14.36	2.52	1.02	0	28.08	29.11	5.31
Oct	0	42.12	10.53	3.37	0.20	9.73	2.22	1.54	0.34	26.21	18.08	5.49
Nov	0	40.55	24.95	4.86	0	10.05	1.61	0.44	0.16	9.78	7.48	4.36
Dec	0	17.05	32.87	10.11	0	7.01	7.20	3.81	0.10	2.54	5.27	6.47

Acknowledgements

This work was jointly supported by the National Natural Science Foundation of China (Grant NOs. 41605042, 41875094, 41605034 and 41501029), the Natural Science Foundation of Jiangsu Province, China (Grant NOs. BK20151525, BK20160948 and BK20150922), the Science Technology Department of Zhejiang Province, China (Grant NO. LGN18D050001), the Qinglan Project of Jiangsu Province of China, and the Priority Academic Program Development (PAPD) of Jiangsu Higher Education Institutions. The source code for the model used in this study and the input files necessary to reproduce the numerical experiments are available from the authors upon request (ppsunsanlei@126.com). The meteorological observations at the 334 weather sites are from the China Meteorological Administration (CMA). Moreover, NCEP Reanalysis data are provided by NOAA/OAR/ESRL PSD, Boulder, Colorado, USA, from https://www.esrl.noaa.gov/psd/ in any documents or publications using these data.

Appendix A. Supplementary data

Supplementary data associated with this article can be found, in the online version, at https://doi.org/10.1016/j.jhydrol.2018.10.071.

References

Allen, C.D., Macalady, A.K., Chenchouni, H., Bachelet, D., McDowell, N., Vennetier, M., Kitzberger, T., Rigling, A., Breshears, D.D., Hogg, E.H., Gonzalez, P., Fensham, R., Zhang, Z., Castro, J., Demidova, N., Lim, J.H., Allard, G., Running, S.W., Semerci, A., Cobb, N., 2010. A global overview of drought and heat induced tree mortality reveals emerging climate change risks for forests. For. Ecol. Manage. 259, 660–684. https://doi.org/10.1016/j.foreco.2009.09.001.

Allen, R.G., Pereira, L.S., Raes, D., Smith, M., 1998. Crop evapotranspiration: guidelines for computing crop requirements, irrigation and drainage paper 56. Roma, Italia.

Bollasina, M.A., Ming, Y., Ramaswamy, V., 2011. Anthropogenic aerosols and the weakening of the South Asian Summer Monsoon. Science 334, 502–505. https://doi.org/10.1126/science.1204994.

Chen, H., Ma, H., Li, X., Sun, S., 2015a. Solar influences on spatial patterns of Eurasian winter temperature and atmospheric general circulation anomalies. J. Geophys. Res. 120. https://doi.org/10.1002/2015JD023415.

Chen, H., Zhang, Y., Yu, M., Hua, W., Sun, S., Li, X., Gao, C., 2015b. Large-scale urbanization effect on eastern Asian summer monsoon circulation and climate. Clim. Dyn. 47, 117–136. https://doi.org/10.1007/s00382-015-2827-3.

Choi, J.-W., Kim, I.-G., Kim, J.-Y., Kim, B.-J., Park, C.-H., Kim, D.-W., 2016. The assessment of droughts in Northern China and Mongolian areas using PDSI and relevant large-scale environments. Int. J. Climatol. 36, 3259–3269. https://doi.org/10.1002/joc.4553.

Cui, H., Zhang, J., Yao, F., 2015. Combination of multi-sensor remote sensing data for drought monitoring over Southwest China. Int. J. Appl. Earth Observ. Geoinf. 35, 270–283. https://doi.org/10.1016/j.jag.2014.09.011.

Dai, A., 2011. Characteristics and trends in various forms of the Palmer Drought Severity Index during 1900–2008. J. Geophys. Res. 116 (D12115). https://doi.org/10.1029/2010JD015541.

Dai, A., 2013. Increasing drought under global warming in observations and models. Nat. Clim. Change 3, 52–58. https://doi.org/10.1038/nclimate1633.

Devaraju, N., Bala, G., Modak, A., 2015. Effects of large-scale deforestation on precipitation in the monsoon regions: remote versus local effects. PNAS 112 (11), 3257–3262. https://doi.org/10.1073/pnas.1423439112.

Diffenbaugh, N.S., Swain, D.L., Touma, D., 2015. Anthropogenic warming has increased drought risk in California. PNAS 112, 3931–3936. https://doi.org/10.1073/pnas.1422385112.

Duan, H., Amthor, J.S., Duursma, R.A., O'Grady, A.P., Choat, B., Tissue, D.T., 2013. Carbon dynamics of eucalypt seedlings exposed to progressive drought in elevated [CO2] and elevated temperature. Tree Physiol. 33, 779–792. https://doi.org/10.1093/treephys/tpt061.

Fan, Z.-X., Thomas, A., 2013. Spatiotemporal variability of reference evapotranspiration and its contributing climatic factors in Yunnan Province, SW China, 1961–2004. Clim. Change 116, 309–325. https://doi.org/10.1007/s10584-012-0479-4.

Feller, U., 2016. Drought stress and carbon assimilation in a warming climate: Reversible and irreversible impacts. J. Plant Physiol. 203, 84–94. https://doi.org/10.1016/j.jplph.2016.04.002.

Ganguli, P., Ganguly, A.R., 2016. Space-time trends in U.S. meteorological droughts. J. Hydrol.: Reg. Stud. 8, 235–259. https://doi.org/10.1016/j.ejrh.2016.09.004.

Gea-Izquierdo, G., Viguera, B., Cabrera, M., Cañellas, I., 2014. Drought induced decline could portend widespread pine mortality at the xeric ecotone in managed Mediterranean pine-oak woodlands. For. Ecol. Manage. 320, 70–82. https://doi.org/10.1016/j.foreco.2014.02.025.

Gray, S.B., Brady, S.M., 2016. Plant developmental responses to climate change. Dev. Biol. 419, 64–77. https://doi.org/10.1016/j.ydbio.2016.07.023.

Guitjens, J.C., 1982. Models of alfalfa yield and evapotranspiration. J. Irrigation Drainage Div. 108, 212–222. https://doi.org/10.1061/(ASCE)0733-9437(1983) 109:3(345).

Harbeck, G.E., 1962. A practical field technique for measuring reservoir evaporation utilizing mass-transfer theory. Geological Survey Professional Paper 272-E, 101–105.

Hobbins, M.T., Dai, A., Roderick, M.L., Farquhar, G.D., 2008. Revisiting the parameterization of potential evaporation as a driver of long-term water balance trends. Geophys. Res. Lett. 35 (L12403). https://doi.org/10.1029/2008GL033840.

Hu, Q., Willson, G.D., 2000. Effect of temperature anomalies on the Palmer drought severity index in the central United States. Int. J. Climatol. 20, 1899–1911. https://doi.org/10.1002/1097-0088(200012)20:15<1899::AID-JOC588>3.0.CO;2-M.

Hua, W., Zhou, L., Chen, H., Nicholson, S.E., Jiang, Y., Raghavendra, A., 2017. Understanding the Central Equatorial African long-term drought using AMIP-type simulations. Clim. Dyn. https://doi.org/10.1007/s00382-017-3665-2.

Huang, Y., Cui, X., 2015. Moisture sources of torrential rainfall events in the Sichuan Basin of China during summers of 2009–13. J. Hydrometeorol. 16, 1906–1917. https://doi.org/10.1175/JHM-D-14-0220.1.

Huang, R., Liu, Y., Wang, L., Wang, L., 2012. Analyses of the causes of severe drought occurring in Southwest China from the fall of 2009 to the spring of 2010. Chin. J. Atmos. Sci. 36, 357–443 (in Chinese with English abstract).

Huang, S., Huang, Q., Chang, J., Zhu, Y., Leng, G., Xing, L., 2015. Drought structure based on a nonparametric multivariate standardized drought index across the Yellow River basin, China. J. Hydrol. 530, 127–136. https://doi.org/10.1016/j.jhydrol.2015.09.042.

IPCC, 2014. Summary for policymakers. In: Field, C.B., Barros, V.R., Dokken, D.J., Mach, K.J., Mastrandrea, M.D., Bilir, T.E., Chatterjee, M., Ebi, K.L., Estrada, Y.O., Genova, R.C., Girma, B., Kissel, E.S., Levy, A.N., MacCracken, S., Mastrandrea, P.R., White, L.L. (Eds.), Climate change 2014: impacts, adaptation, and vulnerability. Part a: global and sectoral aspects. Contribution of working group ii to the fifth assessment report of the intergovernmental panel on climate change. Cambridge University Press, Cambridge, pp. 1–32.

Kalnay, E., Kanamitsu, M., Kistler, R., Collins, W., Deaven, D., Gandin, L., Iredell, M., Saha, S., White, G., Woollen, J., Zhu, Y., Leetmaa, A., Reynolds, B., Chelliah, M., Ebisuzaki, W., Higgins, W., Janowiak, J., Mo, K.C., Ropelewski, C., Wang, J., Roy, Jenne, Joseph, D., 1996. The NCEP/NCAR 40-year reanalysis project. Bull. Am. Meteorol. Soc. 77 (3), 437–470. https://doi.org/10.1175/1520-0477(1996)077<0437:TNYRP>2.0.CO;2.

Kodera, K., Shibata, K., 2006. Solar influence on the tropical stratosphere and troposphere in the northern summer. Geophys. Res. Lett. 33 (L19704). https://doi.org/10.1029/

2006GL026659.
Li, L., Dolman, A.J., Xu, Z., 2016. Atmospheric moisture sources, paths, and the quantitative importance to the Eastern Asian Monsoon Region. J. Hydrometeorol. 17, 637–649. https://doi.org/10.1175/JHM-D-15-0082.1.
Li, Y., Xu, H., Liu, D., 2009. Features of the extremely severe drought in the east of Southwest China and anomalies of atmospheric circulation in summer 2006. Acta Meteorol. Sin. 67 (1), 122–132 (in Chinese with English Abstract).
Li, Z., Feng, Q., Zhang, W., He, Y., Wang, X., Catto, N., An, W., Du, J., Cheng, A., Liu, L., Hu, M., 2012. Decreasing trend of sunshine hours and related driving forces in Southwestern China. Theor. Appl. Climatol. 109, 305–321. https://doi.org/10.1007/s00704-012-0583-4.
Liang, S., Strahler, A.H., Wathall, C., 1998. Retrieval of land surface albedo from satellite observations: a simulation study. J. Appl. Meteorol. Climatol. 38, 712–725. https://doi.org/10.1175/1520-0450(1999) 038<0712:ROLSAF>2.0.CO;2.
Liao, H., Chang, W., Yang, Y., 2015. Climatic effects of air pollutants over China: a review. Adv. Atmos. Sci. 31 (2), 115–139. https://doi.org/10.1007/s00376-014-0013-x.
Liu, B., Chen, X., Lian, Y., Chen, J., Chen, X., 2015a. Long-term change of wet and dry climatic conditions in the southwest karst area of China. Global Planet. Change 127, 1–11. https://doi.org/10.1016/j.gloplacha.2015.01.009.
Liu, B., Li, Y., Chen, J., Chen, X., 2015b. Long-term change in precipitation structure over the karst area of Southwest China. Int. J. Climatol. 36 (6), 2417–2434. https://doi.org/10.1002/joc.4501.
Liu, M., Xu, X., Sun, A., 2015c. Decreasing spatial variability in precipitation extremes in southwestern China and the local/large-scale influencing factors. J. Geophys. Res. 120 (13), 6840–6848. https://doi.org/10.1002/2014JD022886.
Liu, M., Xu, X., Sun, A.Y., Wang, K., 2017a. Decreasing spatial variability of drought in southwest China during 1959–2013. Int. J. Climatol. https://doi.org/10.1002/joc.5109.
Liu, X., Liu, C., Brutsaert, W., 2018. Investigation of a generalized nonlinear form of the complementary principle for evaporation estimation. J. Geophys. Res. 123 (8), 3933–3942.
Liu, X., Li, D., Wang, J., 2012. Spatiotemporal characteristics of drought over China during 1961–2009. J. Desert Res. 32 (2), 473–483 (in Chinese with English abstract).
Liu, X., Xu, X., Yu, M., Lu, J., 2016. Hydrological drought forecasting and assessment based on the standardized stream index in the Southwest China. Procedia Eng. 154, 733–737. https://doi.org/10.1016/j.proeng.2016.07.576.
Liu, Z., Lu, G., He, H., Wu, Z., He, J., 2017b. Anomalous features of water vapor transport during severe summer and early fall droughts in Southwest China. Water 9 (244). https://doi.org/10.3390/w9040244.
Long, D., Shen, Y., Sun, A., Hong, Y., Longuevergne, L., Yang, Y., Li, B., Chen, L., 2014. Drought and flood monitoring for a large karst plateau in Southwest China using extended GRACE data. Remote Sens. Environ. 155, 145–160. https://doi.org/10.1016/j.rse.2014.08.006.
Lu, E., Cai, W., Jiang, Z., Zhang, Q., Zhang, C., Higgins, R.W., Halpert, M.S., 2014. The day-to-day monitoring of the 2011 severe drought in China. Clim. Dyn. 43, 1–9. https://doi.org/10.1007/s00382-013-1987-2.
Lu, E., Luo, Y., Zhang, R., Wu, Q., Liu, L., 2011. Regional atmospheric anomalies responsible for the 2009–2010 severe drought in China. J. Geophys. Res. 116 (D21). https://doi.org/10.1029/2011jd015706.
Ma, M., Ren, L., Singh, V.P., Yuan, F., Chen, L., Yang, X., Liu, Y., 2016. Hydrologic model-based Palmer indices for drought characterization in the Yellow River basin, China. Stoch. Env. Res. Risk Assess. 30, 1401–1420. https://doi.org/10.1007/s00477-015-1136-z.
Mao, R., Gong, D.-Y., Zhao, T., Wang, W., Yang, J., 2015. Trends in the Frequency of high relative humidity over China: 1979–2012. J. Clim. 28, 9816–9836. https://doi.org/10.1175/JCLI-D-14-00840.1.
Marvel, K., Bonfils, C., 2013. Identifying external influences on global precipitation. PNAS 110 (48), 19301–19306.
McKee, T.B., Doesken, N.J., Kleist, J., 1993. The relationship of drought frequency and duration to time steps, preprints. In: 8th conference on applied climatology. Anaheim, CA, 17–22 January 1993, pp. 179–184.
Meir, P., Mencuccini, M., Dewar, R.C., 2015. Drought-related tree mortality: addressing the gaps in understanding and prediction. New Phytologist 207, 28–33. https://doi.org/10.1111/nph.13382.
Milly, P.C., Dunne, K.A., 2016. Potential evapotranspiration and continental drying. Nat. Clim. Change 6, 946–949. https://doi.org/10.1038/nclimate3046.
Mira, M., Weiss, M., Baret, F., Courault, D., Hagolle, O., Gallego-Elvira, B., Olioso, A., 2015. The MODIS (collection V006) BRDF/albedo product MCD43D: temporal course evaluated over agricultural landscape. Remote Sens. Environ. 170, 216–228. https://doi.org/10.1016/j.rse.2015.09.021.
Ning, L., Liu, J., Sun, W., 2017. Influences of volcano eruptions on Asian Summer Monsoon over the last 110 years. Sci. Rep. 7 (42626). https://doi.org/10.1038/srep42626.
Park, S., Feddema, J.J., Egbert, S.L., 2004. Impacts of hydrologic soil properties on drought detection with MODIS thermal data. Remote Sens. Environ. 89, 53–62. https://doi.org/10.1016/j.rse.2003.10.003.
Paschalis, A., Katul, G.G., Fatichi, S., Palmroth, S., Way, D., 2017. On the variability of the ecosystem response to elevated atmospheric CO2, across spatial and temporal scales at the Duke Forest FACE experiment. Agric. For. Meteorol. 232, 367–383. https://doi.org/10.1016/j.agrformet.2016.09.003.
Priestley, C.H.B., Taylor, R.J., 1972. On the assessment of the surface heat flux and evaporation using large-scale parameters. Mon. Weather Rev. 100, 81–92. https://doi.org/10.1175/1520-0493(1972) 100<0081:OTAOSH>2.3.CO;2.
Qin, N., Chen, Fu.G., Zhai, J., Xue, X., 2010. Precipitation and temperature trends for the Southwest China: 1960–2007. Hydrol. Process. 24, 3733–3744. https://doi.org/10.1002/hyp.7792.
Reichstein, M., Bahn, M., Ciais, P., Frank, D., Mahecha, M.D., Seneviratne, S., Zscheischler, J., Beer, C., Buchmann, N., Frank, D.C., Papale, D., Rammig, A., Smith, P., Thonicke, K., van der Velde, M., Vicca, S., Walz, A., Wattenbach, M., 2013. Climate extremes and the carbon cycle. Nature 500, 287–295. https://doi.org/10.1038/nature12350.
Sarojini, B.B., Stott, P.A., Black, E., 2016. Detection and attribution of human influence on regional precipitation. Nat. Clim. Change 6 (7), 669–675. https://doi.org/10.1038/nclimate2976.
Scanlon, B.R., Duncan, I., Reedy, R.C., 2013. Drought and the water-energy nexus in Texas. Environ. Res. Lett. 8 (045033). https://doi.org/10.1088/1748-9326/8/4/045033.
Scott, R.L., Hamerlynck, E.P., Jenerette, G.D., Moran, M.S., Barron-Gafford, G.A., 2010. Carbon dioxide exchange in a semidesert grassland through drought-induced vegetation change. J. Geophys. Res. 115 (G03026). https://doi.org/10.1029/2010JG001348.
Seager, R., Hoerling, M., Schubert, S., Wang, H., Lyon, B., Kumar, A., Nakamura, J., Henderson, N., 2015. Causes of the 2011–14 California drought. J. Clim. 28, 6997–7024. https://doi.org/10.1175/jcli-d-14-00860.1.
She, D., Xia, J., 2013. The spatial and temporal analysis of dry spells in the Yellow River basin, China. Stoch. Env. Res. Risk Assess. 27, 29–42. https://doi.org/10.1007/s00477-011-0553-x.
Sheffield, J., Wood, E.F., Roderick, M.L., 2012. Little change in global drought over the past 60 years. Nature 491, 435–438. https://doi.org/10.1038/nature11575.
Shi, P., Wu, M., Qu, S., Jiang, P., Qiao, X., Chen, X., Zhou, M., Zhang, Z., 2015. Spatial distribution and temporal trends in precipitation concentration indices for the Southwest China. Water Resour. Manage. 29, 3941–3955. https://doi.org/10.1007/s11269-015-1038-3.
Shukla, S., Safeeq, M., AghaKouchak, A., Guan, K., Funk, C., 2015. Temperature impacts on the water year 2014 drought in California. Geophys. Res. Lett. 42. https://doi.org/10.1002/2015GL063666.
Spinoni, J., Naumann, G., Vogt, J.V., 2017. Pan-European seasonal trends and recent changes of drought frequency and severity. Global Planet. Change 148, 113–130. https://doi.org/10.1016/j.gloplacha.2016.11.013.
Sun, Q., Wang, Z., Li, Z., Erb, A., Schaal, C., 2017a. Evaluation of the global MODIS 30 arc-second spatially and temporally complete snow-free land surface albedo and reflectance anisotropy dataset. Int. J. Appl. Earth Observ. Geoinf. 58, 36–49. https://doi.org/10.1016/j.jag.2017.01.011.
Sun, S.L., Chen, H.S., Ju, W.M., Wang, G.J., Sun, G., Huang, J., Ma, H.D., Gao, C.J., Hua, W.J., Yan, G.X., 2017b. On the coupling between precipitation and potential evapotranspiration: contributions to decadal drought anomalies in the Southwest China. Clim. Dyn. 48, 3779–3797. https://doi.org/10.1007/s00382-016-3302-5.
Sun, S.L., Chen, H.S., Ju, W.M., Yu, M., Hua, W.J., Yin, Y., 2014. On the attribution of the changing hydrological cycle in Poyang Lake Basin, China. J. Hydrol. 514, 214–225. https://doi.org/10.1016/j.jhydrol.2014.04.013.
Sun, S.L., Chen, H.S., Sun, G., Ju, W.M., Wang, G.J., Huang, J., Li, X., Gao, C.J., Ma, H.D., 2017c. Attributing the changing reference evapotranspiration in Southwest China using a new separating method. J. Hydrometeorol. 18, 777–798. https://doi.org/10.1175/JHM-D-16-0118.1.
Sun, S.L., Sun, G., Caldwell, P., McNulty, S., Cohen, E., Xiao, J., Zhang, Y., 2015. Drought impacts on ecosystem functions of the U.S. National Forests and Grasslands: Part II assessment results and management implications. For. Ecol. Manage. 353, 269–279. https://doi.org/10.1016/j.foreco.2015.04.002.
Teuling, A.J., Seneviratne, S.I., Stöckli, R., Reichstein, M., Moors, E., Ciais, P., Luyssaert, S., van den Hurk, B., Ammann, C., Bernhofer, C., Dellwik, E., Gianelle, D., Gielen, B., Grünwald, T., Klumpp, K., Montagnani, L., Moureaux, C., Sottocornola, M., Wohlfahrt, G., 2010. Contrasting response of European forest and grassland energy exchange to heatwaves. Nat. Geosci. 3 (10), 722–727. https://doi.org/10.1038/ngeo950.
Teuling, A.J., van Loon, A.F., Seneviratne, S.I., Lehner, I., Marc, A., Heinesch, B., Bernhofer, C., Thomas, G., Heiko, P., Uwe, S., 2013. Evapotranspiration amplifies European summer drought. Geophys. Res. Lett. 40, 2071–2075. https://doi.org/10.1002/grl.50495.
Thornthwaite, C.W., 1948. An approach toward a rational classification of climate. Geogr. Rev. 38, 55–94. https://doi.org/10.2307/210739.
Trenberth, K.E., Dai, A., van der Schrier, G., Jones, P.D., Barichivich, J., Briffa, K.R., Sheffield, J., 2014. Global warming and changes in drought. Nat. Clim. Change 4, 17–22. https://doi.org/10.1038/nclimate2067.
van Loon, H., Meehl, G.A., 2012. The Indian summer monsoon during peaks in the 11-yr sunspot cycle. Geophys. Res. Lett. 39 (L13701). https://doi.org/10.1029/2012GL051977.
Vicente-Serrano, S.M., Beguería, S., López-Moreno, J., 2010. A multiscalar drought index sensitive to global warming: The standardized precipitation evapotranspiration index. J. Clim. 23, 1696–1718. https://doi.org/10.1175/2009JCLI2909.1.
Wang, A., Lettenmaier, D.P., Sheffield, J., 2011. Soil moisture drought in China, 1950–2006. J. Clim. 24, 3257–3271. https://doi.org/10.1175/2011JCLI3733.1.
Wang, H., Chen, Y., Pan, Y., 2015a. Characteristics of drought in the arid region of northwestern China. Clim. Res. 62, 99–113. https://doi.org/10.3354/cr01266.
Wang, H., Lin, H., Liu, D., 2014a. Remotely sensed drought index and its responses to meteorological drought in Southwest China. Remote Sensing Lett. 5, 413–422. https://doi.org/10.1080/2150704X.2014.912768.
Wang, L., Chen, W., 2012. Characteristics of multi-timescale variabilities of the drought over last 100 years in Southwest China. Adv. Meteorol. Sci. Technol. 2 (4), 21–26 (in Chinese with English abstract).
Wang, L., Chen, W., Zhou, W., 2014b. Assessment of future drought in Southwest China based on CMIP5 multimodel projections. Adv. Atmos. Sci. 31, 1035–1050. https://

doi.org/10.1007/s00376-014-3223-3.
Wang, L., Chen, W., Zhou, W., Huang, G., 2015b. Teleconnected influence of tropical Northwest Pacific sea surface temperature on interannual variability of autumn precipitation in Southwest China. Clim. Dyn. 45, 2527–2539. https://doi.org/10.1007/s00382-015-2490-8.
Wei, J., Su, H., Yang, Z.L., 2015. Impact of moisture flux convergence and soil moisture on precipitation: a case study for the southern United States with implications for the globe. Clim. Dyn. 46, 467–481. https://doi.org/10.1007/s00382-015-2593-2.
Wijngaard, J.B., Tank, A.M.G.K., Konnen, G.P., 2003. Homogeneity of 20th century European daily temperature and precipitation series. Int. J. Climatol. 23, 679–692. https://doi.org/10.1002/joc.906.
Wilhite, D., 2000. Drought as a natural hazard: concepts and definitions. In: Wilhite, D.A. (Ed.), Drought: A Global Assessment. Routledge, London, pp. 3–18.
Williams, A.P., Seager, R., Abatzoglou, J.T., Cook, B.I., Smerdon, J.E., Cook, E.R., 2015. Contribution of anthropogenic warming to California drought during 2012–2014. Geophys. Res. Lett. 42, 6819–6828. https://doi.org/10.1002/2015GL064924.
Wu, Z., Mao, Y., Li, X., Lu, G., Lin, Q., Xu, H., 2015. Exploring spatiotemporal relationships among meteorological, agricultural, and hydrological droughts in Southwest China. Stoch. Env. Res. Risk Assess. 30 (3), 1033–1044.
Xu, C.-Y., Singh, V.P., 2001. Evaluation and generalization of temperature-based methods for calculating evaporation. Hydrol. Process. 15, 305–319. https://doi.org/10.1002/hyp.119.
Xu, H., Li, J., Feng, J., Mao, J., 2012. The asymmetric relationship between the winter NAO and the precipitation in Southwest China. Acta Meteorol. Sin. 70 (6), 1276–1291 (in Chinese with English abstract).
Xu, L., Shi, Z., Wang, Y., Zhang, S., Chu, X., Yu, P., 2015. Spatiotemporal variation and driving forces of reference evapotranspiration in Jing River basin, northwest China. Hydrol. Process. 29, 4846–4862. https://doi.org/10.1002/hyp.10541.
Xu, Z., Jiang, Y., Jia, B., Zhou, G., 2016. Elevated-CO_2 response of stomata and its dependence on environmental factors. Front. Plant Sci. 7 (657). https://doi.org/10.3389/fpls.2016.00657.
Yan, G., Wu, Z., Li, D., 2013. Comprehensive analysis of the persistent drought events in Southwest China. Disaster Adv. 6, 306–315.
Yang, J., Gong, D., Wang, S., Hu, M., Mao, R., 2012a. Extreme drought event of 2009/2010 over southwestern China. Meteorol. Atmos. Phys. 115, 173–184. https://doi.org/10.1007/s00703-011-0172-6.
Yang, X., Li, Z., Feng, Q., He, Y., An, W., Wei, Z., Cao, W., Yu, T., Wang, Y., Theakstone, W.H., 2012b. The decreasing wind speed in southwestern China during 1969–2009, and possible causes. Quat. Int. 263, 71–84. https://doi.org/10.1016/j.quaint.2012.02.020.
Yu, M., Li, Q., Hayes, M.J., Svoboda, M.D., Heim, R.R., 2014. Are droughts becoming more frequent or severe in China based on the Standardized Precipitation Evapotranspiration Index: 1951–2010? Int. J. Climatol. 34, 545–558. https://doi.org/10.1002/joc.3701.
Zhai, J., Huang, J., Su, B., Cao, L., Wang, Y., Jiang, T., Fischer, T., 2017. Intensity–area–duration analysis of droughts in China 1960–2013. Clim. Dyn. 48, 151–168. https://doi.org/10.1007/s00382-016-3066-y.
Zhai, J., Su, B., Krysanova, V., Vetter, T., Gao, C., Jiang, T., 2010. Spatial variation and trends in PDSI and SPI indices and their relation to streamflow in large regions of China. J. Clim. 23, 649–663. https://doi.org/10.1175/2009JCLI2968.1.
Zhang, D., Chen, P., Zhang, Q., Li, X., 2017a. Copula-based probability of concurrent hydrological drought in the Poyang lake-catchment-river system (China) from 1960 to 2013. J. Hydrol. 553, 773–784.
Zhang, D., Zhang, Q., Werner, A.D., Liu, X., 2016. GRACE-based hydrological drought evaluation of the Yangtze River Basin, China. J. Hydrometeorol. 17, 811–828. https://doi.org/10.1175/JHM-D-15-0084.1.
Zhang, M., Liu, N., Harper, R., Li, Q., Liu, K., Wei, X., Ning, D., Hou, Y., Liu, S., 2017b. A global review on hydrological responses to forest change across multiple spatial scales: Importance of scale, climate, forest type and hydrological regime. J. Hydrol. 546, 44–59. https://doi.org/10.1016/j.jhydrol.2016.12.040.
Zhang, W., Jin, F.F., Turne, A., 2014. Increasing autumn drought over southern China associated with ENSO regime shift. Geophys. Res. Lett. 41, 4020–4026. https://doi.org/10.1002/2014GL060130.
Zhang, W., Jin, F.-F., Zhan, J.-X., Li, Q., Ren, H.-L., 2013a. The possible influence of a nonconventional El Niño on the severe autumn drought of 2009 in southwest China. J. Clim. 26, 8392–8405. https://doi.org/10.1175/JCLI-D-12-00851.1.
Zhang, W., Jin, F.F., Zhao, J., Qi, L., Ren, H., 2013b. The possible influence of a non-conventional El Niño on the severe autumn drought of 2009 in southwest China. J. Clim. 26, 8392–8405. https://doi.org/10.1175/JCLI-D-12-00851.1.
Zhang, X., Wang, W.C., Fang, X., Ye, Y., Zheng, J., 2012. Agriculture development induced surface albedo changes and climatic implications across northeastern China. Chin. Geograph. Sci. 22, 264–277. https://doi.org/10.1007/s11769-012-0535-z.
Zhao, L., Wang, J.S., Liu, H.W., Xiao, Z., 2017. Amplification of the solar signal in the summer monsoon rainband in China by synergistic actions of different dynamical responses. J. Meteorolog. Res. 31 (1), 61–72. https://doi.org/10.1007/s13351-016-6046-6.
Zou, X., Zhai, P., Zhang, Q., 2005. Variations in droughts over China: 1951–2003. Geophys. Res. Lett. 32 (L04707). https://doi.org/10.1029/2004GL021853.